A Control System for the Reduction of Cargo Pendulation of Ship-Mounted Cranes

Ziyad N. Masoud

Dissertation submitted to the Faculty of the
Virginia Polytechnic Institute and State University
in partial fulfillment of the requirements for the degree of

Doctorate of Philosophy
in
Engineering Science and Mechanics

Ali H. Nayfeh, Chair
Dean T. Mook
Edmund G. Henneke
Scott L. Hendricks
Hugh F. VanLandingham

December 4, 2000
Blacksburg, Virginia

Keywords: Crane control, ship-mounted crane, time-delayed feedback

A Control System for the Reduction of Cargo Pendulation of Ship-Mounted Cranes

Ziyad N. Masoud

(ABSTRACT)

Ship-mounted cranes are used to transfer cargo from large container ships to smaller lighters when deep-water ports are not available. The wave-induced motion of the crane ship produces large pendulations of hoisted cargo and causes operations to be suspended.

In this work, we show that in boom type ship-mounted cranes, it is possible to reduce these pendulations significantly by controlling the slew and luff angles of the boom. Such a control can be achieved with the heavy equipment that is already part of the crane so that retrofitting existing cranes would require a small effort. Moreover, the control is superimposed on the commands of the operator transparently. The successful control strategy is based on delayed-position feedback of the cargo motion in-plane and out-of-plane of the boom and crane tower. Its effectiveness is demonstrated with a fully nonlinear three-dimensional computer simulation and with an experiment on a 1/24 scale model of a T-ACS (The Auxiliary Crane Ship) crane mounted on a platform moving with three degrees of freedom to simulate the ship roll, pitch, and heave motions of the crane ship. The results demonstrate that the pendulations can be significantly reduced, and therefore the range of sea conditions in which cargo-transfer operations could take place can be greatly expanded.

Furthermore, the control strategy is applied experimentally to a scaled model of a tower crane. The effectiveness of the controller is demonstrated for both rotary and gantry modes of operation of the crane.

This work was supported by the Office of Naval Research under Contract #N00014-96-1-1123.

To my Parents

Acknowledgments

First I would like to thank God for his guidance and my parents for their endless love and support. It give me a great honor to thank Dr. Ali Nayfeh and Dr. Dean Mook for their kind support and their patience. I would also like to thank my favorite teacher and my committee member Dr. Scott Hendricks. I also am very grateful to the kindness and continuous encouragement of my other committee members Dr. Edmund Henneke and Dr. Hugh VanLandingham.

I would like to especially thank Sally Shrader for her endless help and patience during the past three years.

I would also like to extend my thanks to all of my friends in the Nonlinear Dynamics and Vibration Research Group, especially Ryan Henry and Eihab Abdel-Rahman. Ryan was the best team mate I have ever worked with. Considering what a disorganized person I am, he had the toughest job of keeping everything in order while doing his share of work. Eihab was always ready to lend a helping hand and guide me through all sorts of problems.

I am especially grateful to my friends Amjad Almousa and Khaled Alhazza. In addition to their unlimited help in the past year, they were the greatest friends and the best company.

Contents

List of Figures

List of Tables

Chapter 1

Introduction

1.1 Introduction

Today ship-mounted cranes are widely used to transfer cargo from large container ships to smaller lighters when deep-water ports are not available. The ships unloaded during these operations include container ships, roll-on/roll-off ships, heavy lift barge carriers, semi-submersible ships, and deep draft tankers. These operations must be suspended when the wave-excited motions of the crane ship produce dangerously large pendulations of the cargo being hoisted.

In the Joint Logistic Over the Shore (JLOTS), JLOTS II, and JLOTS III of the US Army operations, Auxiliary Crane Ships (T-ACS) were used for unloading container ships, Fig 1.1. Once the sea conditions built to a low sea state 3 (as defined by the Piersion-Moskowitz Sea Spectrum with significant wave heights in the range of 1:0 ¡ 1:6m), hoisted payload pendulations on crane ships became dangerously large and the operations had to be suspended [48]. Analysis of worldwide weather and sea-condition data show that

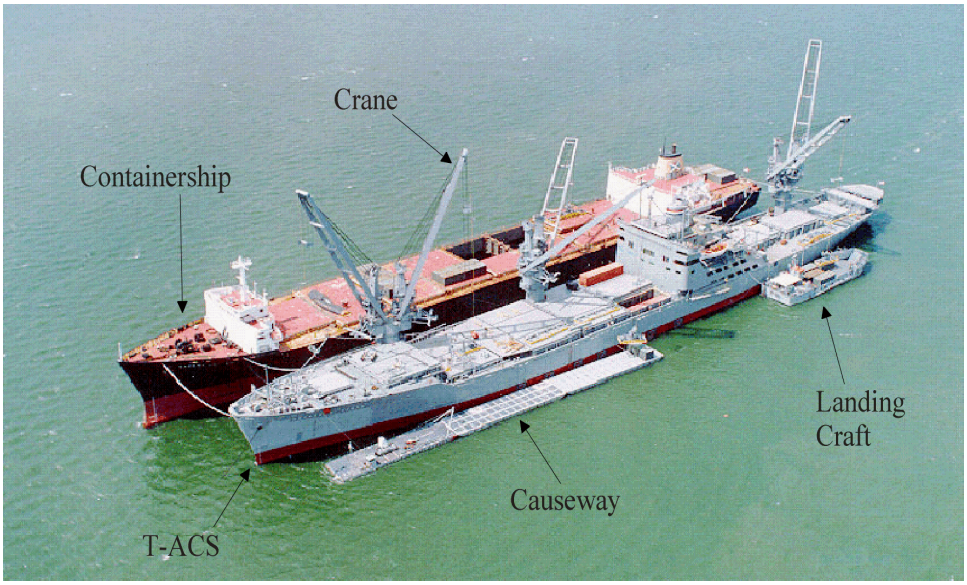

Figure 1.1: Typical T-ACS cargo transfer scenario.

more than 35% of all potential JLOTS sites have sea condition of sea state 3 or higher 50% of the time during which operations would be suspended [48, 49].

Assuming a workability criterion based on the vertical displacement of the boom tip/payload only, Rawston and Blight [39] calculated that a crane vessel in the North Sea could operate only for less than half of its availability time. Nojiri and Sasaki [28] calculated that a barge crane could only be used for heavy lifts in East China Sea for 34% of the time. Their calculations also show that payload pendulations due to excitation frequencies near the resonance frequency of the cable-payload assembly have a pronounced effect on the roll and pitch motions of the crane vessel under the influence of both regular and irregular waves.

Since much time and money can be wasted waiting for acceptable sea conditions, a system to control and reduce the pendulations of the cargo to such an extent that transfer could take place in sea states where these operations are not now possible would be of

tremendous commercial and military value.

The most common type of cranes mounted on crane ships is the boom crane. The issue of crane-payload pendulations using this type of crane has been addressed extensively in a large number of recent studies. Most of these studies were dedicated to land-based cranes and dealt with several issues, such as the automation of the loading and unloading processes, the optimization of the operation time, and the suppression of cargo pendulation resulting from crane-operator input commands. On the other hand, the most important cause of the payload pendulation on ship-mounted cranes is the base excitation due the crane-ship motions. The frequency content of these motions may contain significant energy at/or near the natural frequency and/or twice the natural frequency of the hoisted payload, which could initiate an external and/or a parametric resonance.

1.1.1 Modeling of the Payload-Pendulation Problem

The nature of the payload-pendulation problem was explored in a number of studies. Most of these studies concluded that large load motions necessitates nonlinear analysis of the crane dynamics. One of the first to examine the nonlinearities involved in the dynamic response of a boom crane were Elling and McClinton [9]. They modeled the cable-payload assembly in a ship-mounted boom crane as a spherical pendulum subject to base excitations applied at the boom tip. Using numerical simulation, they solved the equations of motion of the pendulum subject to harmonic base excitations. Their results show a resonant response when the excitation frequency is near the natural frequency (primary resonance) or one-half the natural frequency (secondary resonance) of the assembly. Miles [26, 27] examined the weakly nonlinear response of a lightly damped, spherical pendulum to a simple harmonic, planar displacement of the point of suspension. He found that nonplanar motions could be excited due to the nonlinear interaction

between the two modes of oscillation.

Patel et al. [34], McCormick and Witz [25], and Witz [52] derived a model of a ship-mounted boom crane incorporating the coupled motions of the crane and the ship. Based on computer simulations, they found that "the hook load does not significantly affect the roll motions of the vessel" and that the coupling of ship motions with payload motions has negligible influence on ship motions. A planar model of the in-plane motion of the crane was reduced to a Mathieu equation, thus showing that the load can be parametrically excited due to the vertical motion of the boom tip. Nojiri and Sasaki [28] found that payload pendulations due to an excitation frequency near the resonance frequency of the cable-payload assembly have a pronounced effect on the roll and pitch motions of the crane vessel under the influence of both regular and irregular waves.

Schellin et al. [44] derived a two-dimensional model of a ship-mounted boom crane incorporating the ship surge, heave, and pitch. The ship was modeled as a rigid body, the mooring system as a nonlinear restoring force, and the hoisting cable was allowed to stretch elastically. They found that the natural frequency of the cable-payload assembly in stretching is four orders of magnitude above that in pendulation. They also reported strong coupling between load pendulation and surge and pitch ship motions. Numerical simulations of the system revealed chaos in the response of the load to regular waves at a wave frequency near the natural frequency of the cable-payload assembly and period doubling at frequencies further afield from it. Schellin et al. [43] extended the model to three-dimensions allowing for all ship motions, load pendulations, and damping in the cable. While the model was nonlinear, it assumed small ship rotations. They compared the results of simulations of linear and nonlinear models to the results of experiments on a ship model and found that the nonlinear model was "more realistic" near resonance where large ship and load motions occur. Simulations of the response to wave groups show that payload motions induce ship sway, however the sway does not contribute to

load motions. So it seems likely that the two-dimensional model indication of a coupling between load and ship motions was an artifact of the two-dimensional model. They also found that, when the frequencies of the wave group were close to the natural frequency of the cable-payload assembly, the response was chaotic. They reported that slowly varying low-frequency horizontal ship motions due to the slow component in a wave group did not affect the payload response. Thus, it is a safe assumption to decouple the motions of the crane from those of the ship, lump the ship motion as a base excitation, and apply it to the cable-payload assembly at its point of suspension.

Kral et al. [22] presented a nonlinear planar model of a ship-mounted crane incorporating both the dynamics of the ship and the dynamics of the crane. Computer simulations were employed to explore the impact of cable length changes on payload pendulations. The results showed chaotic behavior at cable lengths over 28 m and multiple responses at the same cable length, depending on whether the cable was reeled or unreeled. Chin et al. [7] derived a three-dimensional nonlinear model of the cable-payload assembly of a ship-mounted crane. They used the model to study crane dynamics due to both direct and parametric external excitations applied at the boom tip. They found that, while the parametric excitation exhibits principal parametric resonance in the neighborhood of twice the natural frequency of the system, the response was always stable, bounded and planar. On the other hand, direct excitations produce complex dynamics when the excitation frequency approaches the natural frequency of the system. They found that a strictly planar excitation could produce in-plane and out-of-plane pendulations, and that the response may exhibit sudden jumps, modulation of the amplitudes and phases (quasi-periodic motion), and chaos.

Posiadala et al. [37] modeled the cable-payload assembly in a truck-mounted boom crane as a spherical pendulum. Base excitations due to the boom slew, luff, and telescopic (extension) motion and forcing due to cable reeling/unreeling were introduced into the

pendulum's equations of motion. Numerical simulations were used to solve for the forced payload response under various motion combinations for 10 s and then its free response for the subsequent 10 s. They found that, except in the absence of slew motion, the payload response is three-dimensional and can not be considered as a planar phenomenon. Posiadala et al. [38] extended the model to account for the flexibility of the cable as a Kelvin-Voigt body. They derived equations of motion describing the position of the payload and the dynamic stretching of the cable. The results showed a fast frequency component in the tension force in the cable, representing the oscillations due to the cable's dynamic stretching. Posiadala [35, 36] extended the work of Posiadala et al. [37] to model a truck crane on an elastic support. He modeled the crane as a rigid body and the supports as elastic springs. He derived equations of motion describing the position of the payload and the position and orientation of the crane. Numerical simulations showed that the free response of the payload is quasi-periodic. The slow frequency in the (in-plane and out-of-plane pendulations) was due to the natural frequency of the cable-payload assembly, while the fast frequency was due to the support response and the resulting base excitations of the system at the boom tip. Towarek [47] derived a model of a truck-mounted boom crane standing on and interacting with a flexible soil. The crane platform was modeled as a rigid body undergoing small oscillations, the boom as a flexible beam, the cable as an elastic string, the cable-payload assembly as a spherical pendulum, and the soil as a viscoelastic Kelvin-Voigt body. He solved the equations of motion of the system for a complete revolution of boom slew at two different speeds. The system response showed that the crane was oscillating with a narrow band of frequencies, thus producing base excitations of the cable-payload assembly at its point of suspension (boom tip).

Ito et al. [16] derived a three-dimensional model of a tuck-mounted boom crane, including the motor, hoisting cables, and a payload. Numerical simulations and experiments were carried for a planar case. They showed that the payload undergoes oscillations due to

longitudinal vibrations in the boom luffing cable and in the payload-hoisting cable. The period of pendulation was one order of magnitude larger than the periods of the cables' longitudinal vibrations.

1.1.2 Control of Payload Pendulation

Many researches investigated control of payload pendulations for fixed-base cranes. The majority of control techniques were developed for gantry cranes. While some controllers were originally designed for boom cranes, others were modifications of earlier work on gantry cranes. Two main approaches can be identified among these researches: one targets pendulation suppression through out the whole transport maneuver, while the other is more concerned with pendulation suppression at the end-of-maneuver, so-called "elimination of residual pendulation". In both approaches, limited research included the operator as a part of the model plant. Lewis et al. [23] and Parker et al. [31] presented a three-dimensional linear model of a boom crane. A controller applies quasi-static filters to the operator's input commands to avoid exciting the natural frequency of the cable-payload assembly. Experimental results showed a significant reduction in both the in-plane and out-of-plane payload pendulations. However, the counter-intuitive delay of all operator inputs continues to exist.

Gustafsson [12] presented a three-dimensional nonlinear model of a boom crane. Two independent, in-plane and out-of-plane, linear position feedback controllers were designed based on a linearization of the model. Computer simulations were conducted. The results showed stable responses for commanded slewing rates away from the natural frequency of the cable-payload assembly. As soon as the ratio of the slewing rate to the natural frequency of the cable-payload assembly approached 1=2, the controller failed due the impact of nonlinearities in the system. Burg et al. [5] reported that the neglected

nonlinearities in a linearized state-space model may significantly impact the performance of the linear controller. Computer simulations showed that a linear controller applied to the system provide an acceptable performance only within a fixed operating range of small pendulation angles around the equilibrium point of the payload.

Hara et al. [13] presented a linear model of a planar telescopic boom crane. To control pendulations due to the telescopic motion of the boom, they designed an LQR controller using the boom telescopic motion as control input. A saturation condition was applied to the controller input to keep it within available control authority. In computer simulations and actual testing, the control strategy was successful in pendulation suppression.

Souissi and Koivo [45] modeled a boom crane as a spherical pendulum. They designed a two-step control scheme. A PID controller to track a reference trajectory using the slew and luff of the boom and the reeling/unreeling of the cable and a PD controller to dampen payload pendulations. Numerical simulation of the boom performing a luffing-slewing-luffing maneuver at constant cable length showed significant payload pendulations, as high as $15^{\pm}$, indicating that the linear controller is not effective in damping pendulations.

Sakawa et al. [41] proposed an optimization scheme that transfers the load to a desired position while minimizing the load swing during the transfer as well as at the end point. The transfer time was minimized by iteration. The technique was applied to models of boom and gantry cranes linearized around the end point of transfer. Sakawa and Nakazumi [40] presented a three-dimensional nonlinear model of a boom crane. An LQR controller employing the slew, luff, and hoisting degrees of freedom as control parameters was developed to eliminate residual pendulations at the end of a predefined maneuver. Computer simulations were conducted to verify the control strategy. The maximum pendulation angle observed during the maneuver was $21{:}6^{\pm}$. Sato and Sakawa [42] extended the model to include an extra jib at the boom tip with a flexible joint.

One of the common recent strategies of controlling payload pendulation without including the operator in the control loop is "Input Shaping". For a predefined endpoint of transport, the input shaping controller drives the suspension point of the payload and the length of the hoist cable along predefined (Shaped) trajectories that avoid exciting payload pendulations. Parker et al. [32, 33] applied this technique to a three-dimensional linear time-varying model of a rotary crane undergoing a jib rotation without a trolley motion. They used optimization techniques to shape the acceleration input of the jib in order to achieve rest-to-rest no-oscillation condition of the payload for a given crane maneuver. Experimental verification of this open-loop controller was conducted. The results showed that significant pendulations developed, reaching as much as $10^{\pm}$ during the given maneuver.

Golafshani and Aplevich [11] presented a nonlinear model of a rotary crane. Time-optimal trajectories of the jib, the trolley, and the cable length were generated. A bang-bang controller was then used to track these trajectories. In computer simulations, the time-optimal trajectories produced uncontrolled payload pendulations. The constraint on the time in the time-optimal trajectories was therefore relaxed to 110% of the optimal value. Trajectories satisfying a minimum payload swing-energy condition were then used. Computer simulations showed that the sub-optimal trajectories reduced the payload pendulations. However, significant pendulations persisted throughout the maneuver and at the end point.

Alsop et al. [2] presented a two-dimensional linear model of a gantry crane. They proposed an input shaping strategy. The proposed controller accelerates in steps of constant acceleration and then kills the acceleration when the load reaches the zero pendulation angle. The same approach is used in the deceleration stage. Computer simulations were conducted using two constant acceleration/deceleration steps. Carbon [6] used two variations of the input shaping technique (one and two-step constant deceleration) of Alsop

et al. to eliminate residual oscillations in a two-dimensional boom crane.

Osinski and Wojciech [30] calculated optimal shapes of input moment or input velocity to the hoist motor during the lifting of a load off a cargo ship by a boom crane. To model the plant, they simplified the model of Koscielny and Wojciech [21] and Osinski and Wojciech [29] by assuming an immobile crane ship and reducing the sea effect on the cargo ship to a harmonic heave motion. They found that including the elasticity of the boom had "only a small influence on load motion."

A limited number of researches approached the issue of payload-pendulation control on ship-mounted cranes, resulting from ship-motion excitation. Iwasaki et al. [17] and Imazeki et al. [15] designed and built an active mass-damper system and installed it on the sling of a barge-mounted boom crane. A two-dimensional linear model of the crane was used to design a linear feedback controller. The input was the acceleration applied to a 35 ton damping mass riding on the sling. A 132 kW induction motor was used to drive the damping mass. Test results showed that the sling motion was reduced to 1=2 to 1=3 of the uncontrolled motions at the same test frequency.

Balachandran and Li [3], Balachandran et al. [4], and Li and Balachandran [24] modified the common boom-crane configuration to suspend the payload from a pivot that in turn was suspended under the boom. The pivot acted as a nonlinear vibration absorber, a mechanical filter, to absorb the cargo oscillations. They derived two-dimensional [3, 4] and three-dimensional [24] models of this new configuration. Their simulations showed that the absorber can suppress subcritical bifurcations and shift the bifurcation points arising from the nonlinear dynamics of the cable-payload assembly.

Yuan et al. [53] presented a new system to rig ship-mounted cranes, Maryland rigging. It transforms a boom crane from a single spherical pendulum to a double pendulum system. The upper pendulum is a pulley riding on a cable suspended from two points on the boom.

Thus, the pulley is constrained to move over an ellipsoid. The lower pendulum is the payload that is suspended by a cable from the pulley, which continues to act as a spherical pendulum. A planar nonlinear model of this rigging was developed. The model response to periodic and chaotic roll motions was investigated. Simulation results showed that the payload response grows significantly in both cases when the period (dominant period for chaotic motion case) approaches the natural frequency of the payload pendulum. The pulley was used as a brake to apply a constant and continuous dry (Coulomb) friction. Results also showed that a friction level equivalent to 10% of the cargo weight reduced the payload pendulation significantly even in the neighborhood of the natural frequency.

Apart from major changes in the crane structure, the Maryland rigging imposes physical constrains on the crane operation, such as reduced reach of the boom and reduced maximum lifting height.

Kimiaghalam et al. [18] applied a fuzzy control approach to the level of Coulomb friction in the Maryland rigging. They also proposed a fuzzy controller to change the damping constant in an active friction adaptation of the Maryland rigging. The performance of the first approach was inferior to the original Maryland rigging setup, while the second was comparable to that of the original Maryland rigging. Kimiaghalam et al. [19] proposed a fuzzy logic controller to change the boom angle and the length of the cable on which the pulley rolls in the Maryland rigging. The performance of the proposed controller was inferior to that of the original Maryland rigging. Kimiaghalam et al. [20] proposed a feedforward controller and applied it to the boom of a Maryland rigged crane to reduce the equilibrium point displacement of the pulley due to the ship rolling. Another feedback controller was added to dampen payload pendulations by changing the length of the pulley cable. The combination was effective in suppressing load pendulations due to ship rolling and initial disturbances. However, the feedback controller assumed full authority on the lengths of the two segments of the pulley cable independently and hence the pulley

position. This totally violates the equations of motion of the system.

Wen et al. [50, 51] linearized the equations of motion of the Maryland rigging. Then, they proposed a feedforward controller and applied it to the length of the pulley cable to cancel the effect of the ship rolling excitation. An LQR feedback controller was then added to the feedforward controller and had the same control input, which was the length of pulley cable. The results showed a pendulation amplitude of $3^{\pm}$. The feedback controller assumes full authority over the position of the pulley, which violates the equations of motion of the system.

Abdel-Rahman and Nayfeh [1] presented a three-dimensional nonlinear model of a boom crane allowing for cable reeling and unreeling. Their simulation showed that a planar direct excitation near the natural frequency applied at the boom tip can produce in-plane and out-of-plane motions, a sudden jump in the response, and a chaotic response as the cable length is changed. They proposed a cable reeling/unreeling scheme to avoid or alleviate these dynamic instabilities.

Most of the existing crane control mechanisms have proven to be inefficient and thus were "locked out and abandoned" by the operators [14]. Input shaping techniques and optimal control techniques require a predetermined endpoint of the transport process. This makes these techniques less practical since most crane operations are coordinated visually by the crane operator. Linear controllers and static feedback linearization control techniques have very poor performance and usually fail due the highly nonlinear nature of the payload oscillations [8].

The majority of the current crane-control strategies are not designed to handle base excitations, and those modified from gantry crane controllers to boom crane controllers have their limitation due to the fact that horizontal motions of the suspension point of the payload cable in the boom plane are very limited when operating at small luff angles. On

the other hand, controllers designed to handle base excitations are still two-dimensional in nature. They are designed to handle payload pendulations in one plane. Pendulations out-of-the controlled plane are not accessible, which make such controllers inefficient in handling general payload pendulations arising either from the direct excitation of payload pendulations in that uncontrolled plane or from the nonlinear interaction between the two oscillation modes of the payload. These control schemes require major modifications to the standard boom-crane structure and are very complicated to apply.

1.2 Objective

The objective of this work is to use the concept of delayed-position feedback to develop a control system to reduce pendulations of hoisted cargos on ship-mounted cranes to such an extent that cargo transfer could take place in sea states where these operations are now not possible. The controller should require no major modifications to the current boom-crane structure and should be designed to operate transparently to the crane operator. This would eliminate any special training requirements for crane operators and would furnish smoother and faster transport operations.

1.3 Approach

We started with a comprehensive survey of the literature available on the control of boom cranes. A mathematical model including geometric and kinetic nonlinearities was developed. The mathematical model was then solved numerically to analyze its nonlinearities.

A delayed-position feedback controller was developed. In theory, delayed-position feed-

back produces damping in the system; consequently, there is the expectation that the oscillations amplitudes will be significantly reduced, which will make it possible to operate shipboard cranes in higher sea states than is currently possible. The stability of the controlled mathematical model was analyzed. The controller was then applied to a boom crane via standard luff and slew crane inputs. To verify that the controlled system will function as expected, we simulated on a computer the cargo transfer operation with a controlled crane. Results of numerical simulations of the controlled model are presented.

The proposed control system was applied to a 1=24 scale model of the crane currently in use on Keystone State Class Auxiliary Crane Ships (T-ACS), Fig 1.1. We mounted the crane model on a platform that can execute prescribed motions in heave, pitch, and roll, which are the most important components of the general motion of a ship and we tested the controlled model crane under sea states 3 and higher. Loading and unloading operations under these sea states were demonstrated.

Furthermore, the control strategy was applied to, and tested on, an experimental scale model of a land-based tower crane. The control input was introduced through the rotary and gantry degrees of freedom of the crane. The controlled crane was tested in both rotary and gantry modes of operation.

Chapter 2

Dynamics of Hoisted Payload

2.1 Mathematical Model

Experiments by Todd et al. [46] as well as our conducted experiments showed that a ship-mounted boom crane exhibits the typical dynamic behavior of a forced spherical pendulum, including chaotic and/or nonplanar responses to strictly planar excitations at frequencies near the natural frequency of the payload pendulation. In this work, the model used to develop the controller was a spherical pendulum with an inextensible massless cable and a massive point load, as shown in Fig 2.1. Points P and Q represent the boom tip and the load, respectively. The cable length is L_c.

To describe the orientation of the cable with respect to the inertial frame $(x; y; z)$, we use a sequence of two angles, represented by μ_x and μ_y in Fig 2.1. These two angles will be referred to as the in-plane and out-of-plane pendulation angles of the pendulum, respectively. We begin with the cable aligned parallel to the z-axis and then rotate it

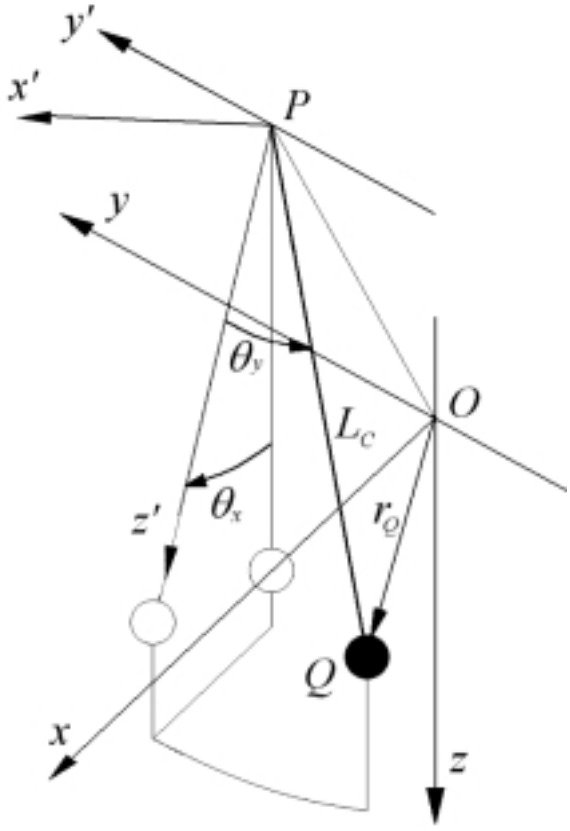

Figure 2.1: A schematic diagram of the cargo and hoisting cable model.

through the angle μ_x around an axis through P that is parallel to the inertial y-axis. This step forms the $(x^0; y^0; z^0)$ coordinate system. Finally, we rotate the cable about the newly formed x^0-axis through the angle μ_y. The position of point P in the inertial frame is given by $(x_p(t); y_p(t); z_p(t))$. It follows that the inertial position r_Q of Q is given by

$$\begin{aligned} r_Q = [x_p(t) + \sin(\mu_x(t))\cos(\mu_y(t))L_c]i + [y_p(t) \ i \ \sin(\mu_y(t))L_c]j \\ +[z_p(t) + \cos(\mu_x(t))\cos(\mu_y(t))L_c]k \end{aligned} \tag{2.1}$$

The equations of motion of this spherical pendulum, which include terms to account for the friction and air resistance, are

$$\begin{aligned}
&[\ddot{\mu}_x(t) + 2\dot{\mu}_x(t)]\cos(\mu_y(t)) - 2\sin(\mu_y(t))\dot{\mu}_x(t)\dot{\mu}_y(t) + \frac{g}{L_c}\sin(\mu_x(t)) \\
&+\frac{1}{L_c}\cos(\mu_x(t))[\ddot{x}_p(t) + 2\dot{x}_p(t)] - \frac{1}{L_c}\sin(\mu_x(t))[\ddot{z}_p(t) + 2\dot{z}_p(t)] = 0
\end{aligned} \tag{2.2}$$

$$\begin{aligned}
&\ddot{\mu}_y(t) + 2\dot{\mu}_y(t) + \sin(\mu_y(t))\cos(\mu_y(t))\dot{\mu}_x^2(t) + \frac{g}{L_c}\cos(\mu_x(t))\sin(\mu_y(t)) \\
&- \frac{1}{L_c}\sin(\mu_x(t))\sin(\mu_y(t))[\ddot{x}_p(t) + 2\dot{x}_p(t)] - \frac{1}{L_c}\cos(\mu_y(t))[\ddot{y}_p(t) + 2\dot{y}_p(t)] \\
&- \frac{1}{L_c}\cos(\mu_x(t))\sin(\mu_y(t))[\ddot{z}_p(t) + 2\dot{z}_p(t)] = 0
\end{aligned} \tag{2.3}$$

where ζ is assumed to be the combined coefficient of joint friction and air resistance.

Cranes are typically lightly damped. Todd et al. [46] report that a ship-mounted boom crane has a damping of 0:1% to 0:5% of the critical damping.

2.2 Analysis of Spherical-Pendulum Behavior with Base Excitation

To analyze the behavior of a payload suspended from a crane, we solve the dynamic equations of motion (2.2) and (2.3) of the spherical pendulum. Due to the complex nonlinearity of these equations, we use numerical techniques to solve for and analyze their behavior.

To find the most critical excitation scenario, we rescale the variables in the equations of motion as follows:

$$\mu_x(t) = {}^2\mu_x(t) \tag{2.4}$$

$$\mu_y(t) = {}^2\mu_y(t) \tag{2.5}$$

$$x_p(t) = {}^2x_p(t) \tag{2.6}$$

$$y_p(t) = {}^2y_p(t) \tag{2.7}$$

$$z_p(t) = {}^2z_p(t) \tag{2.8}$$

where ^{2} is a small nondimensional quantity, which is a measure of the amplitude of the motion. The rescaled variables are then substituted into the nonlinear equations of motion (2.2) and (2.3), and the equations are then expanded. Keeping terms up to order ^{22}, we find that the equations of motion become

$$\ddot{\mu}_x(t) + 2{}^1\dot{\mu}_x(t) + \frac{g}{L_c}\mu_x(t) + \frac{1}{L_c}[\ddot{x}_p(t) + 2{}^1\dot{x}_p(t)] - \frac{{}^2}{L_c}\mu_x(t)[\ddot{z}_p(t) + 2{}^1\dot{z}_p(t)] = 0 \tag{2.9}$$

$$\ddot{\mu}_y(t) + 2{}^1\dot{\mu}_y(t) + \frac{g}{L_c}\mu_y(t) - \frac{1}{L_c}[\ddot{y}_p(t) + 2{}^1\dot{y}_p(t)] - \frac{{}^2}{L_c}\mu_y(t)[\ddot{z}_p(t) + 2{}^1\dot{z}_p(t)] = 0 \tag{2.10}$$

Because the terms involving $x_p(t)$ and $y_p(t)$ appear as additive terms in the rescaled equations of motion (2.9) and (2.10), the most critical conditions occur when their frequencies are approximately equal to the natural frequency $!_n$ of the spherical pendulum. And because the terms involving $z_p(t)$ appear as multiplicative terms in the rescaled equations of motion, the most critical conditions occur when the frequency of the $z_p(t)$ is approximately equal to twice the natural frequency of the spherical pendulum. Hence, to simulate the behavior of the spherical pendulum under the most critical conditions, we excited the suspension point of the pendulum $(x_p(t); y_p(t); z_p(t))$ sinusoidally in the x- and y-directions at the natural frequency of the pendulum and sinusoidally in the z-direction at twice the natural frequency of the pendulum; that is we let

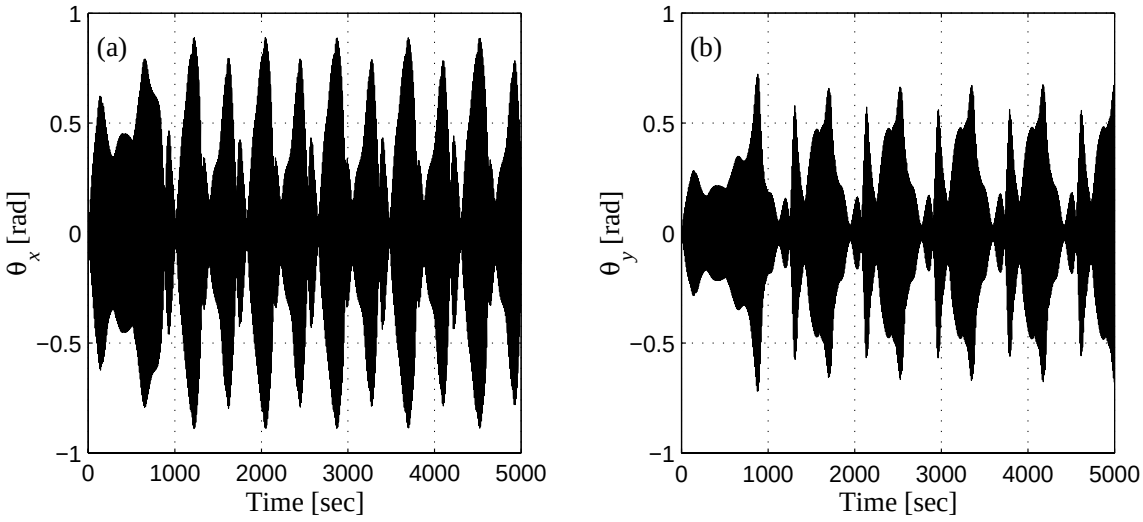

Figure 2.2: Numerical simulation results of the (a) in-plane and the (b) out-of-plane pendulation angles of a spherical pendulum with base excitation at the natural pendulation frequency in the x- and y-directions and at twice the natural pendulation frequency in the z-direction.

$$x_p(t) = A_x \sin(\omega_n t) \tag{2.11}$$

$$y_p(t) = A_y \sin(\omega_n t) \tag{2.12}$$

$$z_p(t) = A_z \sin(2\omega_n t) \tag{2.13}$$

These excitations are substituted into the nonlinear equations of motion (2.2) and (2.3), and the resulting equations are then solved numerically for a long period of time. For the purpose of numerically solving these equations, we choose a spherical pendulum with a linear period of 10 seconds ($L_c = 24{:}849$ m) and damping factor of 0:007. The amplitudes A_x, A_y, and A_z of the base excitations are chosen to be 0:5 m, 0:25 m, and 0:125 m respectively. Results of the numerical solution are shown in Fig 2.2.

Studying Fig 2.2, we notice that the system takes relatively very long time to reach steady state, from which we conclude that a controller design process should not be based on

the steady-state response of the spherical pendulum. We also observe that, although the excitation magnitude in the x-direction is twice as large as that in the y-direction, both in-plane and out-of-plane motions of the hoisted payload grow to the same order of magnitude due to the nonlinear interaction between the in-plane and out-of-plane modes of oscillation. This means that a smaller excitation amplitude or an excitation that is away from the natural frequency of the pendulum in one plane does not necessarily mean that the amplitude of the response in that direction would not grow to a higher amplitude.

Another observation in Fig 2.2 is that the nonlinear interaction between the in-plane and the out-of-plane modes is relatively slow. This means that a controller designed to absorb the oscillation energy from one mode would not be efficient in absorbing energy from the other mode due to the slower rate of energy transfer between the two modes.

Analyzing the frequency content of the response, we make an irrelevant but interesting observation in that the system response seams to be quasi-periodic, Fig 2.3. A Poincare

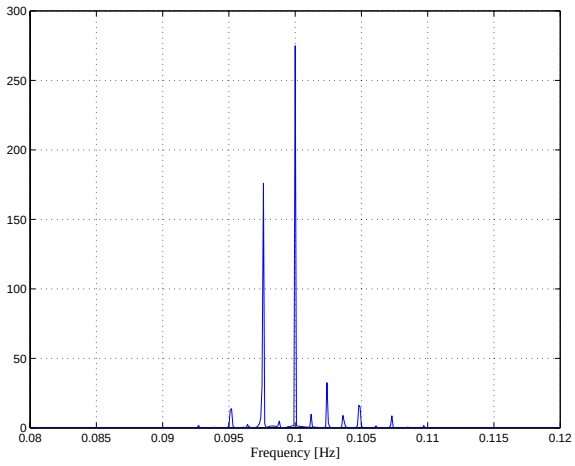

Figure 2.3: Frequency content of a spherical-pendulum response with base excitation at the natural pendulation frequency in the x- and y-directions and at twice the natural pendulation frequency in the z-direction.

section taken at the natural period of the pendulum shows a clearer picture of the quasiperiodic nature of the pendulum response, Fig 2.4.

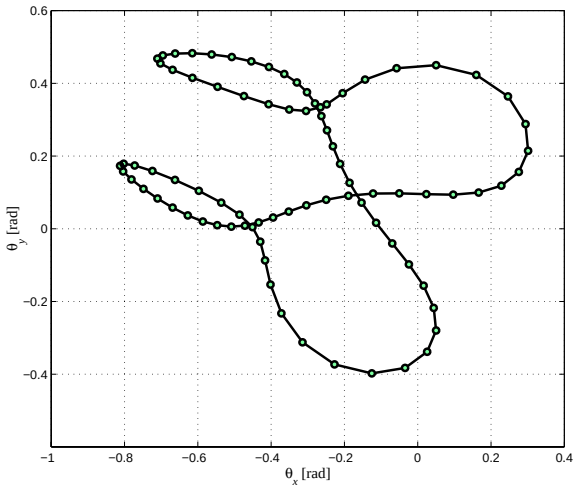

Figure 2.4: A Poincare section of a spherical-pendulum response with base excitation at the natural pendulation frequency in the x- and y-directions and at twice the natural pendulation frequency in the z-direction.

Chapter 3

Controller Design and Analysis

3.1 Delayed-Position Feedback

In theory, delayed feedback in a controlled system produces damping in the system response; consequently, there is the expectation that the oscillation amplitude of a crane payload, represented by a spherical pendulum, will be significantly suppressed by forcing the suspension point of the payload hoisting cable to track inertial reference coordinates $(x_{ref}(t), y_{ref}(t))$. These reference coordinates consist of a percentage of the delayed motion of the payload in the inertial horizontal plane, relative to that suspension point, superimposed on fixed or slowly varying inertial input coordinates $(x_i(t), y_i(t))$. The $(x_i(t), y_i(t))$ coordinates are defined by the crane operator. A tracking controller is used to ensure proper tracking of the desired $(x_{ref}(t), y_{ref}(t))$ coordinates of the suspension point.

This control concept applies to all types of cranes that use a cable for the purpose of

hoisting and transferring cargo. To apply our control concept to our model of the payload hoisting cable assembly, represented by a spherical pendulum, we actuate the suspension point of the hoisting cable in the x- and y-directions. These two degrees of freedom already exist in most crane types. The operator commands are transformed into the desired $(x_i(t), y_i(t))$ coordinates of the suspension point of the hoisting cable.

The horizontal motion of the payload relative to the suspension point of the hoisting cable can be measured using several techniques, including a Global Positioning System (GPS), accelerometers, and inertial encoders that measure angles of the payload hoisting cable. Based on measurements of the angles of the payload hoisting cable, as shown in Fig 2.1, the delay control law takes the following form:

$$x_{ref}(t) = x_i(t) + k_x L_c \cos(\mu_y(t - \zeta_x)) \sin(\mu_x(t - \zeta_x)) \tag{3.1}$$

$$y_{ref}(t) = y_i(t) - k_y L_c \sin(\mu_y(t - \zeta_y)) \tag{3.2}$$

where k_x and k_y are the controller gains and ζ_x and ζ_y are the time delays. The time delay in the feedback loop of the controller creates the required damping effect in the system. A set of two PD tracking controllers is used to apply this control algorithm to ensure that the suspension point of the payload follows the prescribed reference position.

3.2 Stability Analysis

To obtain the equations of motion of the controlled system, we substitute the reference coordinates $(x_{ref}(t), y_{ref}(t))$, Eqs. (3.1) and (3.2), for the suspension point coordinates $(x_p(t), y_p(t))$ into Eqs. (2.2) and (2.3), and obtain the following equations of motion for the controlled system:

$$
\begin{aligned}
&[\ddot{\mu}_x(t) + 2\zeta\dot{\mu}_x(t)]\cos(\mu_y(t)) - 2\sin(\mu_y(t))\dot{\mu}_x(t)\dot{\mu}_y(t) + \frac{1}{L_c}\cos(\mu_x(t))[\ddot{x}_i(t) + 2\zeta\dot{x}_i(t)] \\
&- \frac{1}{L_c}\sin(\mu_x(t))[\ddot{z}_p(t) + 2\zeta\dot{z}_p(t)] + \frac{g}{L_c}\sin(\mu_x(t)) + k_x\cos(\mu_x(t))\cos(\mu_x(t-\tau_x)) \\
&[\ddot{\mu}_x(t-\tau_x) + 2\zeta\dot{\mu}_x(t-\tau_x)]\cos(\mu_y(t-\tau_x)) - 2\dot{\mu}_x(t-\tau_x)\dot{\mu}_y(t-\tau_x)\sin(\mu_y(t-\tau_x)) \\
&- k_x\cos(\mu_x(t))\sin(\mu_x(t-\tau_x)) \\
&[\ddot{\mu}_y(t-\tau_x) + 2\zeta\dot{\mu}_y(t-\tau_x)]\sin(\mu_y(t-\tau_x)) + [\dot{\mu}_x^2(t-\tau_x) + \dot{\mu}_y^2(t-\tau_x)]\cos(\mu_y(t-\tau_x)) = 0
\end{aligned}
\tag{3.3}
$$

$$
\begin{aligned}
&\ddot{\mu}_y(t) + 2\zeta\dot{\mu}_y(t) + \sin(\mu_y(t))\cos(\mu_y(t))\dot{\mu}_x^2(t) - \frac{1}{L_c}\sin(\mu_x(t))\sin(\mu_y(t))[\ddot{x}_i(t) + 2\zeta\dot{x}_i(t)] \\
&- \frac{1}{L_c}\cos(\mu_y(t))[\ddot{y}_i(t) + 2\zeta\dot{y}_i(t)] - \frac{1}{L_c}\cos(\mu_x(t))\sin(\mu_y(t))[\ddot{z}_p(t) + 2\zeta\dot{z}_p(t)] \\
&+ \frac{g}{L_c}\cos(\mu_x(t))\sin(\mu_y(t)) - k_x\sin(\mu_x(t))\sin(\mu_y(t))\cos(\mu_x(t-\tau_x)) \\
&[\ddot{\mu}_x(t-\tau_x) + 2\zeta\dot{\mu}_x(t-\tau_x)]\cos(\mu_y(t-\tau_x)) - 2\dot{\mu}_x(t-\tau_x)\dot{\mu}_y(t-\tau_x)\sin(\mu_y(t-\tau_x)) \\
&+ k_x\sin(\mu_x(t))\sin(\mu_y(t))\sin(\mu_x(t-\tau_x)) \\
&[\ddot{\mu}_y(t-\tau_x) + 2\zeta\dot{\mu}_y(t-\tau_x)]\sin(\mu_y(t-\tau_x)) + [\dot{\mu}_x^2(t-\tau_x) + \dot{\mu}_y^2(t-\tau_x)]\cos(\mu_y(t-\tau_x)) \\
&- k_y\cos(\mu_y(t)) \\
&\dot{\mu}_y^2(t-\tau_y)\sin(\mu_y(t-\tau_y)) - [\ddot{\mu}_y(t-\tau_y) + 2\zeta\dot{\mu}_y(t-\tau_y)]\cos(\mu_y(t-\tau_y)) = 0
\end{aligned}
\tag{3.4}
$$

Equations (3.3) and (3.4) are the equations of motion of a controlled spherical pendulum with a time-delayed position feedback controller.

To analyze the stability of the response of the controlled equations of motion, we scale the variables of the system into fast-varying and slowly-varying terms and analyze the stability of the fast-varying dynamics. The fast-varying terms are

$$\mu_x(t) = \epsilon\mu_x(t) \tag{3.5}$$

$$\mu_y(t) = \epsilon\mu_y(t) \tag{3.6}$$

$$z_p(t) = \epsilon z_p(t) \tag{3.7}$$

and the slowly-varying terms are

$$x_i(t) = \epsilon^2 x_i(t) \tag{3.8}$$

$$y_i(t) = \epsilon^2 y_i(t) \tag{3.9}$$

where ϵ is a small nondimensional quantity, which is a measure of the amplitude of the motion.

Substituting Eqs. (3.5)-(3.9) into Eqs. (3.3) and (3.4) and setting the coefficients of ϵ equal to zero, we obtain

$$\ddot{\mu}_x(t) + 2\epsilon\zeta\dot{\mu}_x(t) + \frac{g}{L_c}\mu_x(t) + k_x\ddot{\mu}_x(t - \tau_x) + 2\epsilon\zeta k_x\dot{\mu}_x(t - \tau_x) = 0 \tag{3.10}$$

$$\ddot{\mu}_y(t) + 2\epsilon\zeta\dot{\mu}_y(t) + \frac{g}{L_c}\mu_y(t) + k_y\ddot{\mu}_y(t - \tau_y) + 2\epsilon\zeta k_y\dot{\mu}_y(t - \tau_y) = 0 \tag{3.11}$$

Since both Eq. (3.10) and (3.11) are mathematically identical, we solve Eq. (3.10). The same conclusions will apply to Eq. (3.11). We seek the solution of Eq. (3.10) in the form

$$\mu_x(t) = ae^{\sigma t}\cos(\omega t + \mu_o) \tag{3.12}$$

where a, σ, ω, and μ_o are real constants. Substituting Eq. (3.12) into Eq. (3.10) and setting each of the coefficients of $\sin(\omega t+\mu_o)$ and $\cos(\omega t+\mu_o)$ equal to zero independently, we obtain

$$k(\sigma^2 + 2\zeta\sigma - \omega^2)\sin(\omega\tau) - 2k\omega(\zeta + \sigma)\cos(\omega\tau) - 2\omega(\sigma + \zeta)e^{\sigma\tau} = 0 \quad (3.13)$$

$$2k\omega(\zeta + \sigma)\sin(\omega\tau) + k(\sigma^2 + 2\zeta\sigma - \omega^2)\cos(\omega\tau) + (\sigma^2 + 2\zeta\sigma - \omega^2 + \frac{g}{L_c})e^{\sigma\tau} = 0 \quad (3.14)$$

For a given gain k and delay time τ, Eqs. (3.13) and (3.14) can be solved for ω and σ. Then, a and μ_0 are determined from initial conditions.

The stability of the system depends on the variable σ. The system is stable when $\sigma < 0$ and unstable when $\sigma > 0$. The boundaries of stability correspond to $\sigma = 0$. To determine these boundaries, we substitute $\sigma = 0$ into Eqs. (3.13) and (3.14) and obtain

$$k\omega^2\sin(\omega\tau) + 2k\zeta\omega\cos(\omega\tau) + 2\zeta\omega = 0 \quad (3.15)$$

$$2k\omega\zeta\sin(\omega\tau) - \omega^2(1 + k\cos(\omega\tau)) + \Omega^2 = 0 \quad (3.16)$$

where $\Omega = \sqrt{g/L_c}$ is the natural pendulation frequency of the payload. Equations (3.15) and (3.16) are nondimensionalized by dividing them by Ω^2 and setting the time delay τ proportional to the uncontrolled natural pendulation period T. The result is

$$k\eta^2\sin(2\pi\eta\varepsilon) + 2k\zeta\eta\cos(2\pi\eta\varepsilon) + 2\zeta\eta = 0 \quad (3.17)$$

$$2k\zeta\eta\sin(2\pi\eta\varepsilon) - \eta^2(1 + k\cos(2\pi\eta\varepsilon)) + 1 = 0 \quad (3.18)$$

where $\eta = \omega/\Omega$, $\varepsilon = \tau/T$, and $\zeta = \zeta/\Omega$. Varying ε and solving Eqs. (3.17) and (3.18) for η and k, we determine the stability boundaries. Figure 3.1 shows the stability boundaries as a function of the relative time delay ε and the controller gain k for a relative damping $\zeta = 0.0033$. The unshaded region corresponds to the stable response region.

Varying τ and k in Eqs. (3.13) and (3.14), we determine the magnitude σ of damping resulting from each gain-delay combination. Figure 3.2 shows contours of the damping

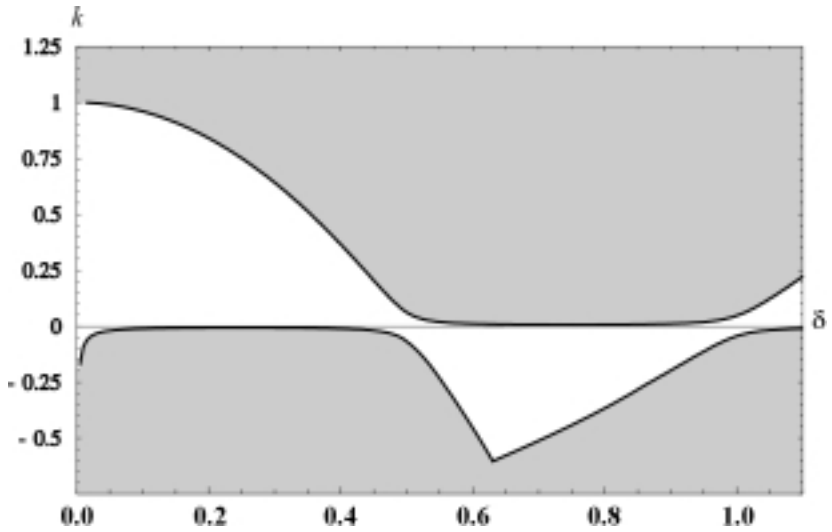

Figure 3.1: Stability diagram of the delay controller. The unshaded area is the stable region.

variable ¾. The darker the shade is, the higher the damping is. This figure is later used in the controller design process to select the best gain-time-delay combination.

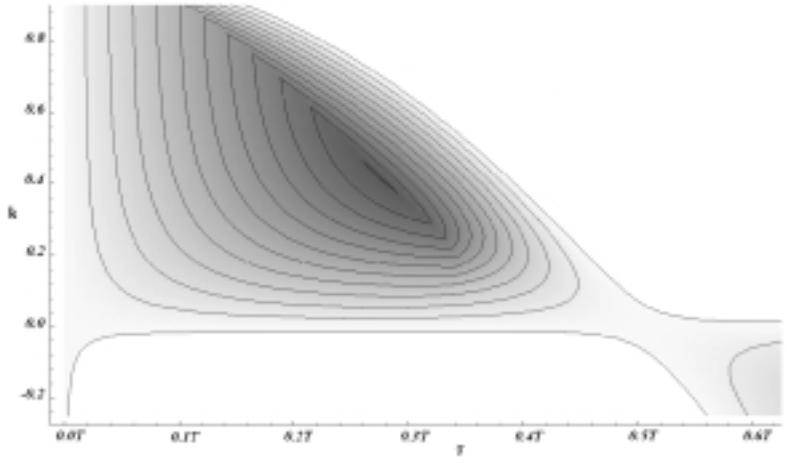

Figure 3.2: A contour plot of the damping as a function of k and ¿, where ¿ is given in terms of the natural period T of the uncontrolled system. The darker areas correspond to higher damping.

3.3 Controller Design for a Ship-Mounted Crane

Simultaneous activation of the luff and slew angles in boom cranes gives the suspension point (boom tip) of the payload pendulum the freedom to move to any prescribed horizontal position within reach of the boom of the crane. Applying the delayed-position feedback controller to these motions can reduce the payload pendulation in- and out-of-the plane formed by the boom and crane tower. The luff and slew degrees of freedom already exist in ship-mounted boom cranes; therefore, no major modifications to the existing structure of the cranes are required. Modifications would be limited to the addition of a few sensors to provide readings of the pendulation angles of the payload hoisting cable, crane luff and slew angles, and the motion of the crane ship. A personal computer, a programmable control board, or a chip to be programmed and added to the crane's computer, if it has one, would be used to apply the control law.

To apply the delayed-position feedback control algorithm, we use a set of two PD tracking controllers to drive the boom luff and slew angles. The operator input commands are routed through the delayed-position feedback controller to the PD controllers, thereby functioning transparently to the operator. The crane actuators are assumed to be strong enough to move the boom rapidly to satisfy the reference luffing and slewing signals at the end of each sampling period. Therefore, in the design process of the controller, we take into consideration the speed limits on the luffing and slewing degrees of freedom of the crane to make sure that the controller does not impose unexecutable conditions on the crane actuators.

For a boom crane with luffing and slewing degrees of freedom, mounted on a ship that is swaying, surging, heaving, pitching, and rolling, as shown in Fig 3.3, point O is a reference point in the ship where the sway $w(t)$, surge $u(t)$, and heave $¡h(t)$ motions of the ship are measured [10]. It coincides with the origin of the inertial reference coordinate

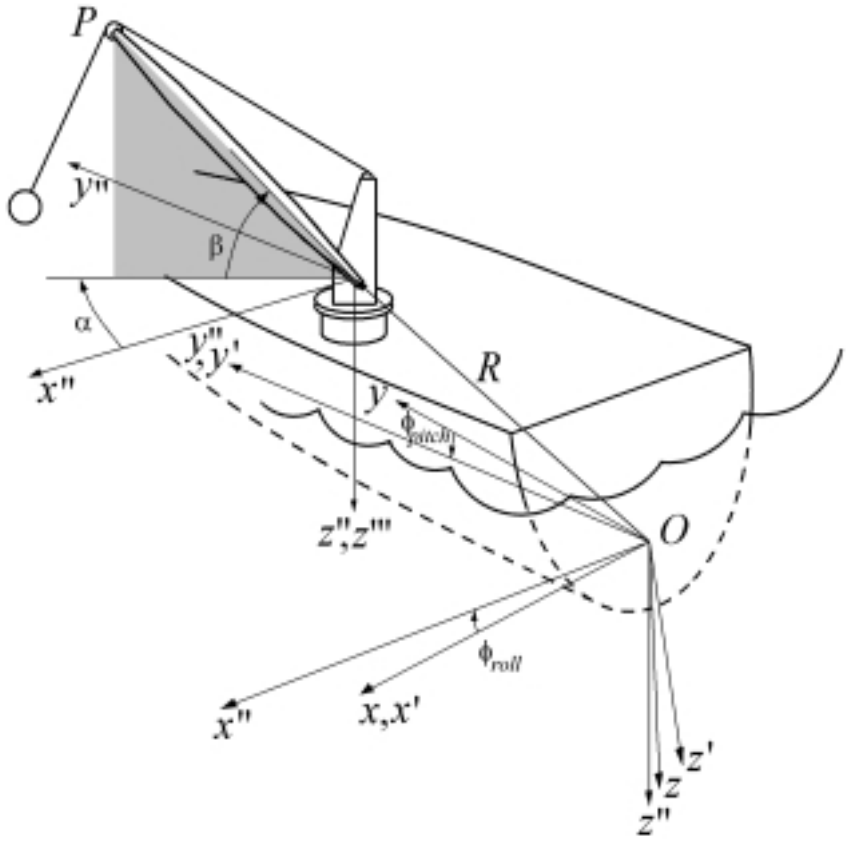

Figure 3.3: A ship-mounted boom crane: $(x; y; z)$ is an inertial coordinate system and $(x^{00}; y^{00}; z^{00})$ is a ship-fixed coordinate system.

system when the ship is stationary. To describe the inertial position of the boom tip, the sway, surge, and heave motions we measure at point O. We use a sequence of Euler angles to determine the orientation of the ship in space. A ship-fixed coordinate system at point O pitches around the inertial x-axis through the angle $Á_{pitch}$ to form the $(x^0; y^0; z^0)$ coordinate system, then it rolls around the newly formed y^0-axis through the angle $Á_{roll}$ to form the $(x^{00}; y^{00}; z^{00})$ coordinate system. Using these measurements, we can give the inertial coordinates of the boom tip as follows:

$$\begin{bmatrix} x_p(t) \\ y_p(t) \\ z_p(t) \end{bmatrix} = \begin{bmatrix} w(t) \\ u(t) \\ -h(t) \end{bmatrix} + \begin{bmatrix} 1 & 0 & 0 \\ 0 & \cos(\phi_{pitch}(t)) & -\sin(\phi_{pitch}(t)) \\ 0 & \sin(\phi_{pitch}(t)) & \cos(\phi_{pitch}(t)) \end{bmatrix} \begin{bmatrix} \cos(\phi_{roll}(t)) & 0 & \sin(\phi_{roll}(t)) \\ 0 & 1 & 0 \\ -\sin(\phi_{roll}(t)) & 0 & \cos(\phi_{roll}(t)) \end{bmatrix} \begin{bmatrix} R_x \\ R_y \\ R_z \end{bmatrix} + \begin{bmatrix} L_b \cos(\gamma(t)) \cos(\theta(t)) \\ L_b \cos(\gamma(t)) \sin(\theta(t)) \\ -L_b \sin(\gamma(t)) \end{bmatrix}, \tag{3.19}$$

where L_b is the boom length and $R = (R_x; R_y; R_z)$ is the position of the boom base relative to the point O and is described in the ship-fixed coordinate system $(x''; y''; z'')$. The inertial horizontal coordinates of the boom tip are

$$\begin{aligned} x_p(t) = w(t) &+ \cos(\phi_{roll}(t))(R_x + \cos(\theta(t)) \cos(\gamma(t)) L_b) \\ &+ \sin(\phi_{roll}(t))(R_z - \sin(\gamma(t)) L_b) \end{aligned} \tag{3.20}$$

$$\begin{aligned} y_p(t) = u(t) &+ \cos(\phi_{pitch}(t))(R_y + \sin(\theta(t)) \cos(\gamma(t)) L_b) \\ &+ \sin(\phi_{pitch}(t)) \sin(\phi_{roll}(t))(R_x + \cos(\theta(t)) \cos(\gamma(t)) L_b) \\ &- \sin(\phi_{pitch}(t)) \cos(\phi_{roll}(t))(R_z + \sin(\gamma(t)) L_b) \end{aligned} \tag{3.21}$$

First, the controller converts the operator luffing $\gamma_i(t)$ and slewing $\theta_i(t)$ commands into an inertial reference target position $(x_i(t), y_i(t))$ of the boom tip. This can be done in any arbitrary way. As an example, we use the trajectory of the boom tip corresponding to the operator commanded luffing $\gamma_i(t)$ and slewing $\theta_i(t)$ for a stationary ship; that is,

$$x_i(t) = R_x + L_b \cos(\gamma_i(t)) \cos(\theta_i(t)) \tag{3.22}$$

$$y_i(t) = R_y + L_b \cos(\gamma_i(t)) \sin(\theta_i(t)) \tag{3.23}$$

where $\bar{}_i(t)$ and $®_i(t)$ are obtained by integrating the operator-commanded luffing and slewing rates. Forcing the boom tip to track these inertial $x_i(t)$ and $y_i(t)$ coordinates minimizes the horizontal excitations on the boom tip resulting from the ship motion. A percentage of the time-delayed payload motion in the inertial xy-plane derived from the time-delayed in-plane and out-of-plane pendulation angles of the payload is then superimposed on the $x_i(t)$ and $y_i(t)$ inputs of the operator to form the commanded boom-tip position $(x_{ref}(t), y_{ref}(t))$ in the inertial reference system. The result is

$$\begin{aligned} x_{ref}(t) = x_i(t) &+ k_{in} L_c \sin(\mu_{in}(t - ¿_{in})) \cos(\mu_{out}(t - ¿_{in})) \cos(®(t)) \\ &+ k_{out} L_c \sin(\mu_{out}(t - ¿_{out})) \sin(®(t)) \end{aligned} \tag{3.24}$$

$$\begin{aligned} y_{ref}(t) = y_i(t) &+ (k_{in} L_c \sin(\mu_{in}(t - ¿_{in})) \cos(\mu_{out}(t - ¿_{in}))) \sin(®(t)) \\ &- (k_{out} L_c \sin(\mu_{out}(t - ¿_{out}))) \cos(®(t)) \end{aligned} \tag{3.25}$$

where μ_{in}, the inertial in-plane pendulation angle, has replaced μ_x, and μ_{out}, the inertial out-of-plane pendulation angle, has replaced μ_y to account for the crane slewing angle ®, as shown in Fig 3.4. Here, k_{in} and k_{out} are the controller gains and $¿_{in}$ and $¿_{out}$ are the time delays. As shown in the preceding section, these time-delayed components produce the damping required to suppress the residual pendulations.

The controller replaces $(x_p(t); y_p(t))$ in Eqs. (3.20) and (3.21) with $(x_{ref}(t), y_{ref}(t))$ and solves for luff and slew angles $(®(t), \bar{}(t))$ with respect to the ship-fixed coordinate system. The final part of the controller consists of two tracking PD controllers, which rapidly drive the boom luff and slew actuators to track the reference angles $\bar{}(t)$ and $®(t)$.

A block diagram of the delayed-position feedback control system applied to a ship-mounted crane is shown in Fig 3.5. The figure shows the controller inputs and outputs with a schematic of the signal processing stages. Steps 300 to 304 are performed using

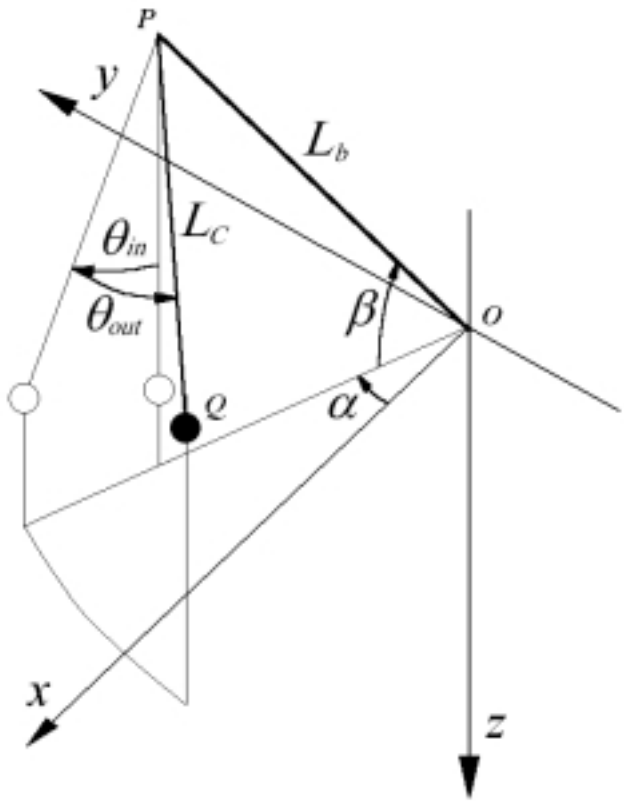

Figure 3.4: Luff and slew angles and in-plane and out-of-plane pendulation angles.

Eqs. (3.22) and (3.23), steps 306 through 316 are performed using the controller main equations (3.24) and (3.25). Step 320 utilizes the readings of the ship-motion sensors 318 to calculate the boom reference luff and slew angles using Eqs. (3.20) and (3.21). Two tracking controller, 324 and 328, are then used to control the boom luff and slew actuators by forcing them to track the reference luff and slew signals of the delayed-position feedback controller.

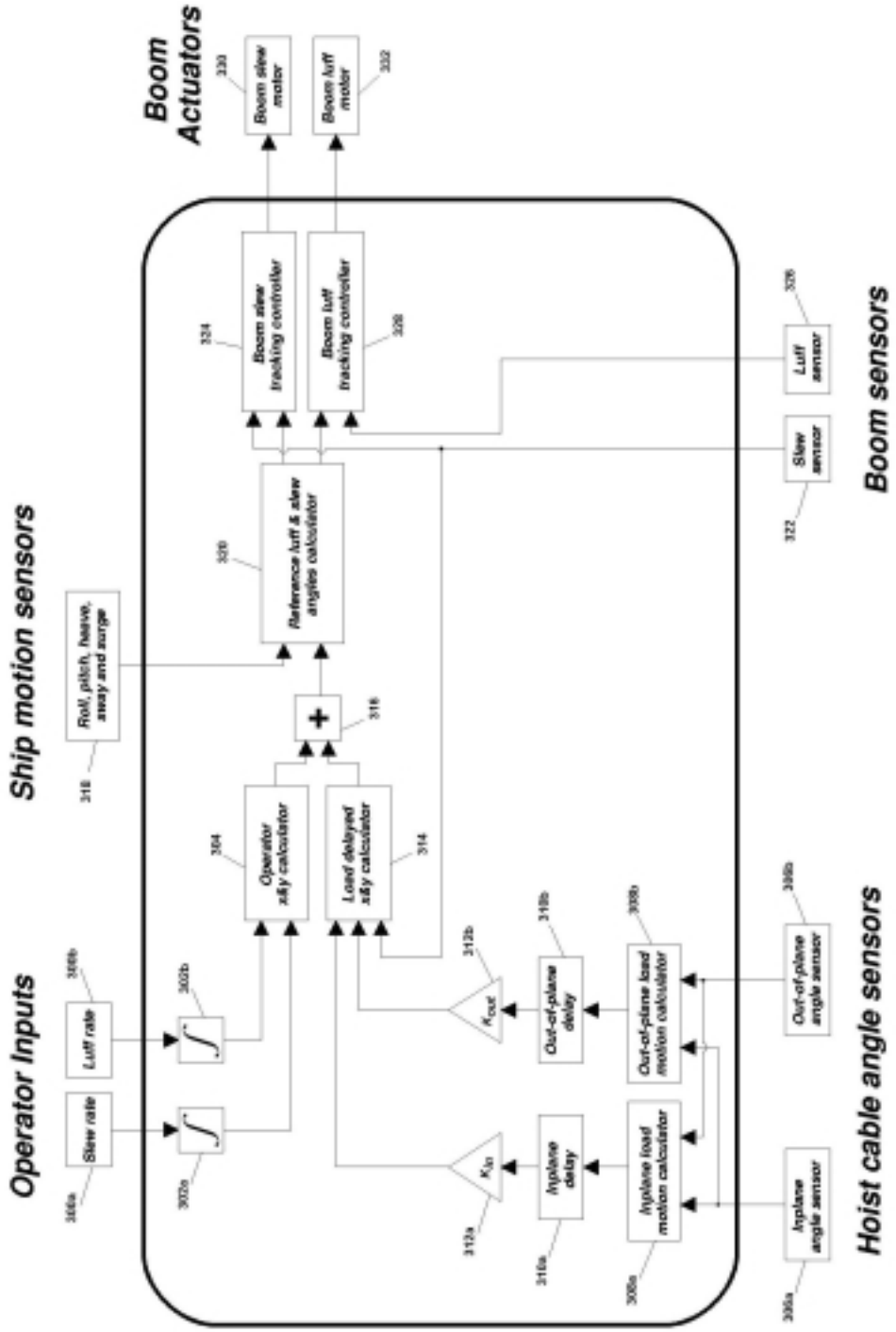

Figure 3.5: A block diagram of the delayed-position feedback controller for a ship-mounted crane.

3.4 Controller Design for a Tower Crane

In tower cranes, the suspension point of the payload pendulum has the freedom to move to any prescribed horizontal position within the reach of the crane using the crane's rotational and translational degrees of freedom. Applying the delayed-position feedback controller to these motions can reduce the payload pendulation in- and out-of-the plane formed by the jib and crane tower.

To apply the delayed-position feedback control algorithm, we use two PD tracking controllers to drive the actuators of the rotating jib and the moving trolley. As it was previously done in the design process of the ship-mounted crane controller, the operator input commands are routed through the delayed-position feedback controller to the PD controllers, thereby functioning transparently to the operator. The crane actuators are assumed to be strong enough to move the jib and the trolley rapidly to satisfy the reference rotation and translation signals at the end of each sampling period. Again, the limits on the crane actuators' speeds are taken into consideration in the process of designing the delayed-position feedback controller.

For a land-based tower crane Fig 3.6, point O is a reference point at the base of the crane. To describe the inertial position of the suspension point of the payload hoisting cable (trolley, P), both rotational and translational positions of the jib and trolley are measured. Using these measurements, we can give the inertial horizontal coordinates of the trolley as follows:

$$x_p(t) = r(t)\cos(®(t)) \tag{3.26}$$

$$y_p(t) = r(t)\sin(®(t)) \tag{3.27}$$

where $r(t)$ is the trolley radial position and $®(t)$ is the rotational position of the jib.

The operator rotation and translation commands ($r_i(t)$, $\theta_i(t)$) are transformed into an inertial reference target position ($x_i(t)$, $y_i(t)$) of the trolley using Eqs. (3.26) and (3.27). Using Eqs. (3.24) and (3.25), we superimpose a percentage of the time-delayed payload motion in the xy-plane derived from the time-delayed in-plane and out-of-plane pendulation angles of the payload on the $x_i(t)$ and $y_i(t)$ inputs of the operator to form the commanded trolley position ($x_{ref}(t)$, $y_{ref}(t)$) in the inertial reference system. Using these reference inertial coordinates and Eqs. (3.26) and (3.27), we obtain reference rotation and translation signals ($r_{ref}(t)$, $\theta_{ref}(t)$). The final part of the controller consists of two tracking PD controllers, which rapidly drive the jib and trolley of the crane to track the reference rotation and translation signals ($r_{ref}(t)$, $\theta_{ref}(t)$).

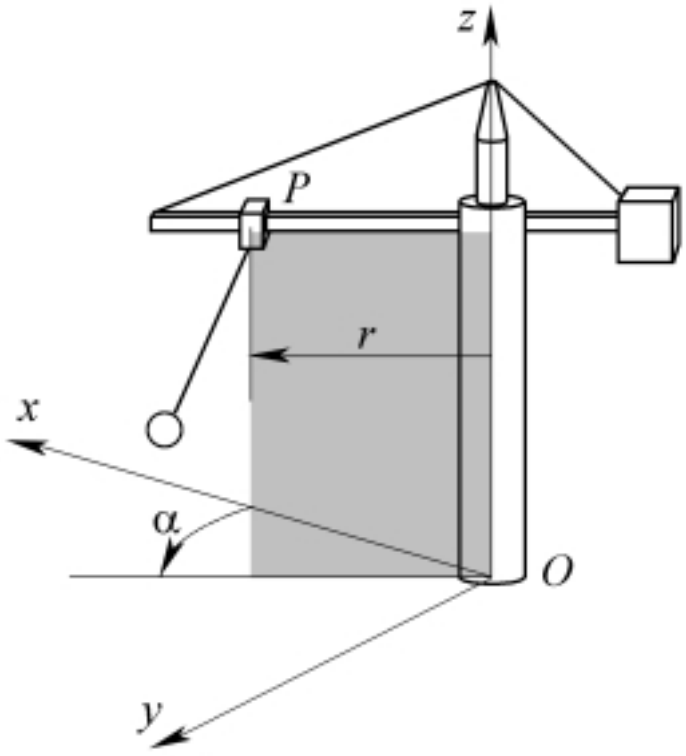

Figure 3.6: A model of tower crane.

Chapter 4

Computer Simulations

4.1 Computer Model

A three-dimensional computer model was constructed based on the dimensions of the T-ACS crane ship, which are given in Table 4.1. In these simulations, we chose crane location 2. Figure 4.1 shows a drawing of the geometry of the computer model. The center of gravity of the hoisted cargo is 27:1m below the boom tip, making the natural frequency of the payload pendulation 0:096 Hz. A linear damping factor of 0:002 was used. An inextensible massless rigid link was used to model the hoisting cable. The payload is excited via primary resonance and principal parametric resonance by setting the frequencies of the rolling and pitching motions of the ship equal to the natural frequency of the payload pendulation and the frequency of the heaving motion equal to twice the natural frequency of the payload pendulation. These conditions are the worst-case excitation as explained earlier. In the computer simulations, we used these conditions to demonstrate the effectiveness of the controller.

Table 4.1: Dimensions of the T-ACS ship and crane. All dimensions are in ft.

Ship Dimension	LBP	633
	Beam	76
	KG	21.81
	GM	9.42
Crane 1 Location	Fwd of Midships	192
	Stbd of Centerline	25
	Waterline at Bottom of Slew Ring	69 above keel
Crane 2 Location	Fwd of Midships	59.5
	Stbd of Centerline	27.17
	Waterline at Bottom of Slew Ring	69.83 above keel
Crane 3 Location	Aft of Midships	233
	Stbd of Centerline	27.17
	Waterline at Bottom of Slew Ring	71.00 above keel
Crane Dimension	Boom Length	121

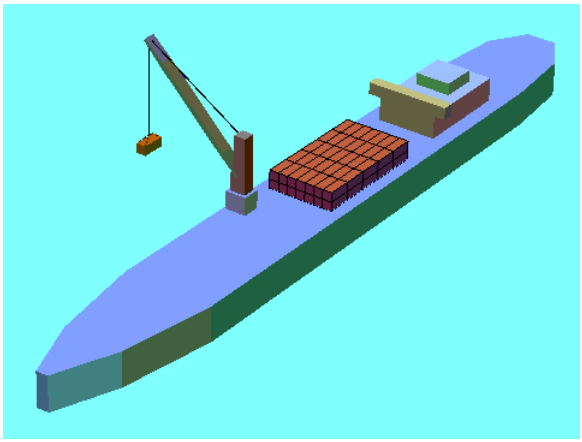

Figure 4.1: Computer model geometry of the T-ACS ship and crane.

A time delay of 2:5 seconds was chosen for the in-plane and out-of-plane angles of the payload cable, which is about 1=4th the pendulation period of the uncontrolled payload pendulum. A gain of 0:1 was used for both the in-plane and out-of-plane parts of the controller. The roll amplitude was $2^{\pm}$, the pitch amplitude was $1^{\pm}$, and the heave amplitude was 0:305m, both controlled and uncontrolled cases were simulated.

4.2 Numerical Simulations

Three sets of simulations were performed. In the first set, the crane was oriented so that the boom was extended over the side of the ship perpendicular to its axis. The boom luff angle was set equal to $45^{\pm}$. The results of the controlled and uncontrolled in-plane and out-of-plane angles of the hoisting cable are shown in Fig 4.2. In the uncontrolled simulation, the pendulation angles of the payload hoisting cable grew rapidly

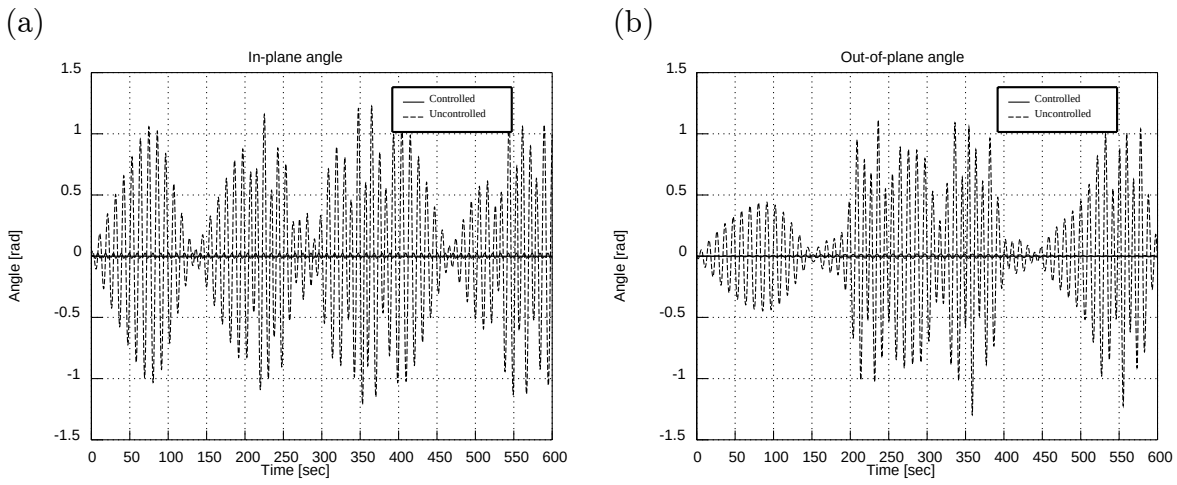

Figure 4.2: Computer simulations: (a) in-plane and (b) out-of-plane angles of the payload cable as functions of time. Sinusoidal excitations in roll and pitch at the natural frequency of the payload pendulation and sinusoidal excitation in heave at twice the natural frequency of the payload pendulation.

to approximately $70^{\pm}$ in-plane and $65^{\pm}$ out-of-plane. On the other hand, the controlled response remained within $1{:}5^{\pm}$ in-plane and $1^{\pm}$ out-of-plane.

The luffing and the slewing actions imposed by the controller on the boom are shown in Fig 4.3. The maximum luffing rate was less than $1^{\pm}$=sec while the maximum slewing rate was less than $0{:}5^{\pm}$=sec. These rates are very reasonable and are within the luffing and slewing capability of most ship-mounted boom cranes.

At the beginning of the second set of simulations, the crane was oriented so that the boom was extended over the side of the ship perpendicular to its axis. The boom luff angle was set equal to $45^{\pm}$. The controller was turned off, and the crane operator executed a sinusoidal slewing action through $90^{\pm}$ and back in every 40 seconds. The same simulation was then repeated with the controller turned on. The results of the controlled and uncontrolled in-plane and out-of-plane angles of the hoisting cable are shown the Fig 4.4. The payload pendulation in the uncontrolled simulation grew rapidly to approximately

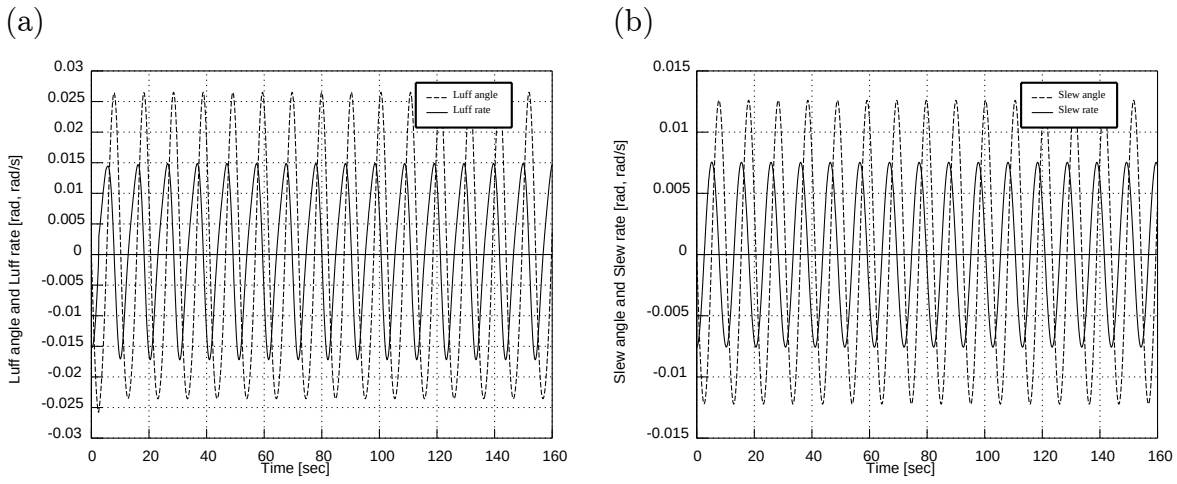

Figure 4.3: Computer simulations: Controller commanded (a) luffing, and (b) slewing actions as functions of time. Sinusoidal excitations in roll and pitch at the natural frequency of the payload pendulation and sinusoidal excitation in heave at twice the natural frequency of the payload pendulation.

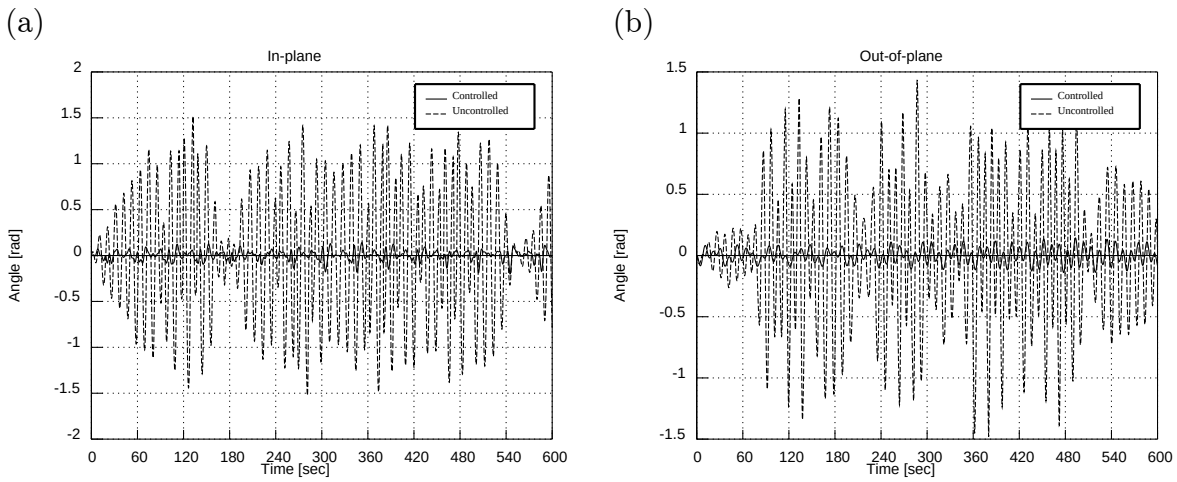

Figure 4.4: Computer simulations: (a) in-plane and (b) out-of-plane angles of the payload cable as functions of time. Sinusoidal excitations in roll and pitch at the natural frequency of the payload pendulation and sinusoidal excitation in heave at twice the natural frequency of the payload pendulation, while the crane was performing a slewing action through $90^{\pm}$ and back every 40 seconds.

$85^{\pm}$ in-plane and $80^{\pm}$ out-of-plane; while in the controlled simulation the pendulation angles remained within $8^{\pm}$ both in-plane and out-of-plane.

To demonstrate the robustness of the controller, in the final set of simulations, the crane was oriented so that the boom was extended over the side of the ship and normal to the ship axis. The boom luff angle was set equal to $45^{\pm}$. The payload position was given a $60^{\pm}$ in-plane initial disturbance. The crane was subjected to the same roll, pitch, and heave excitations as in the two previous simulations. The results of the controlled and uncontrolled in-plane angle of pendulation of the payload are shown in Fig 4.5. While the uncontrolled response grew to approximately $100^{\pm}$, the controlled response dropped rapidly and remained within $2^{\pm}$.

In the controlled simulations, the input power to the crane luff and slew actuators was about 20% higher than the input power required to perform the same operation without

the controller.

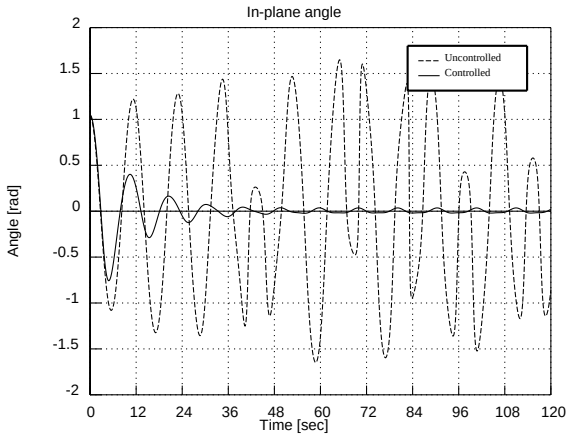

Figure 4.5: Computer simulations: in-plane angle of the payload cable as a function of time. Sinusoidal excitations in roll and pitch at the pendulation frequency of the payload, sinusoidal excitation in heave at twice the pendulation frequency of the payload, and an initial disturbance of $60^{\pm}$ in the in-plane angle.

Chapter 5

Experimental Validation

5.1 Experimental Setup for Ship-Mounted Cranes

To validate the theory and the computer simulations, we built an experimental setup. A 1=24 scale model of a T-ACS crane was mounted on the moving platform of a Carpal wrist mechanism, as shown in Fig 5.1. A rotary platform with a 1 : 45 gear ratio was used to give the crane its slewing degree of freedom.

The platform used is capable of producing arbitrary independent roll, pitch, and heave motions. A desktop computer supplies the rolling, pitching, and heaving commands to the platform motors. The platform was driven to simulate the motion of the crane ship at the crane location 2, the same crane location used for the computer simulations. A digital tilt sensor was fitted to the platform to measure the platform roll and pitch angles.

The crane model was equipped with two brushless servo-motors to actuate the boom in luff and slew. A third motor was added to actuate the payload hoisting for future

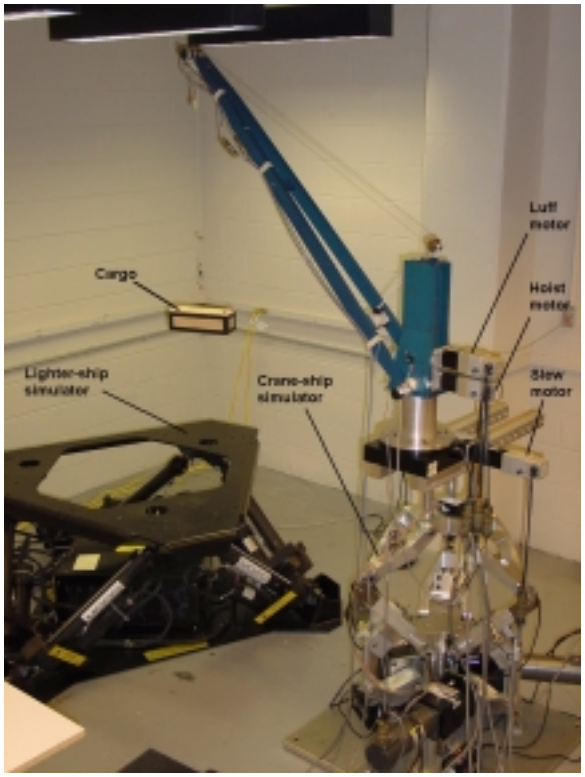

Figure 5.1: A 1=24 scale model of the T-ACS crane mounted on the three-degrees-of-freedom Carpal wrist platform used to simulate the ship motion.

experiments. Two optical encoders were mounted at the boom tip to read the in-plane and out-of-plane angles of the payload hoisting cable. Another optical encoder was mounted at the boom pivot to provide the boom luff angle, and a fourth optical encoder embedded in the servo-motor driving the slewing degree of freedom of the crane was used to measure the slewing angle of the crane. A 1=24 scale model of an 8 ft by 8 ft by 20 ft container weighing 20 tons was used as a payload. The center of gravity of the payload was located 1 m below the boom tip. This length yields a pendulation frequency of 0:498 Hz.

A data acquisition board was added to a 450 MHz desktop computer. The board has 8 channels of analog inputs, 8 channels of analog outputs, 8 encoder counters, and 32

channels of digital inputs/outputs. The board was used to sample the crane encoders and the platform digital tilt sensor. A C++ code was developed to sample the data registers of the acquisition board and drive the amplifiers of the boom luff and slew actuators. The delayed-position feedback control algorithm was added to the code in a way that it could be turned on and off at any time during the experiment. A number of safety limit switches were placed on the crane and were continuously monitored by both the amplifiers of the crane actuators and the C++ code through the data acquisition board.

5.2 Experimental Results for Ship-Mounted Cranes

Experiments were carried out for the worst-case scenario of sinusoidal motions at the critical frequencies. Through out these experiments, the platform and the crane model were excited sinusoidally by $2^{\pm}$ in roll at the pendulation frequency (0:498 Hz), by $1^{\pm}$ in pitch at the pendulation frequency, and by 1:27cm in heave at twice the pendulation frequency. The controller parameters used were a time delay of 0:5 seconds for the in-plane and out-of-plane angles of the payload hoisting cable, which was about 1=4th the pendulation period of the model payload, and a gain of 0:1 for both the in-plane and out-of-plane parts of the controller.

Two sets of experiments were conducted. In both sets, controlled and uncontrolled cases were run. In the first set of experiments, the crane model was extended over the side of the modeled ship and perpendicular to its axis. The boom luff angle was set equal to $45^{\pm}$. In the uncontrolled case, as shown in Fig 5.2, the excitation caused the amplitude of the pendulation angles to grow rapidly, and the experiment had to be stopped at 10 seconds when the in-plane pendulation angle reached approximately $70^{\pm}$. The same experiment was then repeated with the controller turned on. The maximum amplitude of the in-plane and out-of-plane pendulation angles remained less than $1{:}5^{\pm}$ and $2^{\pm}$, respectively.

(a) (b)

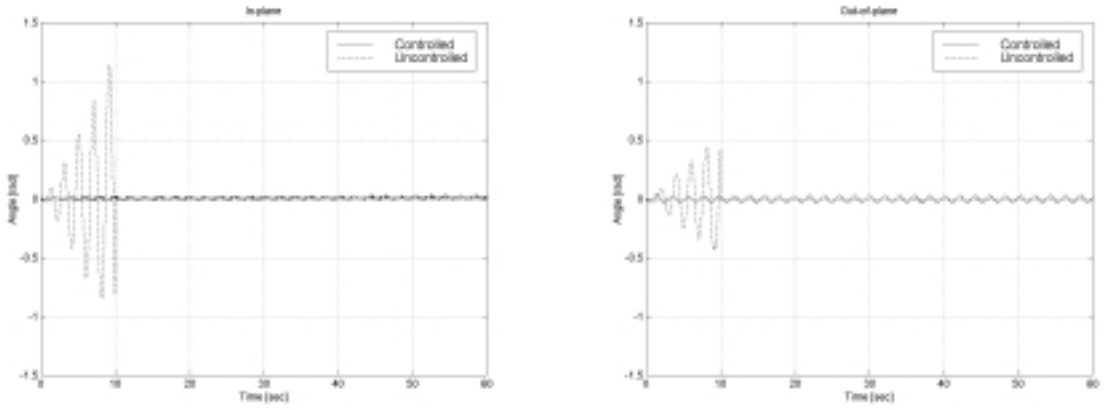

Figure 5.2: Experimental results: (a) in-plane and (b) out-of-plane angles of the payload cable as functions of time. Sinusoidal excitations in roll and pitch at the pendulation frequency of the payload and sinusoidal excitation in heave at twice the pendulation frequency of the payload.

In the second set of experiments, the crane model was initially extended over the side of the modeled ship and perpendicular to its axis. The boom luff angle was set equal to $45^{\pm}$. The crane operator performed a sinusoidal slewing action from $0^{\pm}$ to $90^{\pm}$ in every 8 seconds. In the uncontrolled case, as shown in Fig 5.3, the excitation together with the slewing action caused the amplitude of the pendulation angles to grow rapidly, and the experiment had to be stopped at 10 seconds when the in-plane pendulation angle reached approximately $70^{\pm}$. The same experiment was then repeated with the controller turned on. The maximum amplitude of the in-plane and out-of-plane pendulation angles remained less than $6^{\pm}$.

An additional experiment was conducted. The experiment started with the controller turned off. After a few seconds, and when the in-plane pendulation angle of the payload had increased to over $20^{\pm}$, the controller was turned on. This was done to simulate the influence of initial disturbances. After the controller was turned on, the pendulation angles of the payload dropped in 10 seconds and remained less than $1^{\pm}$, as shown in

Fig 5.4.

(a) (b)

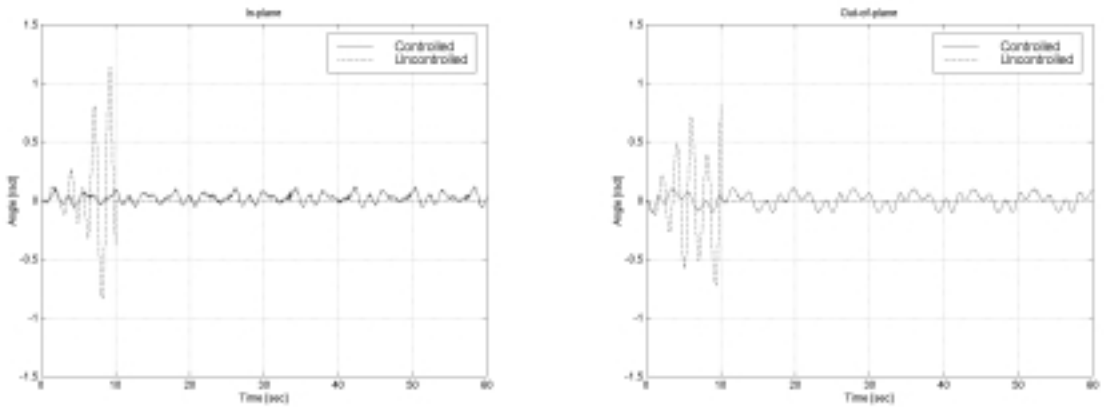

Figure 5.3: Experimental results: (a) in-plane and (b) out-of-plane angles of the payload cable as functions of time. Sinusoidal excitations in roll and pitch at the pendulation frequency of the payload and sinusoidal excitation in heave at twice the pendulation frequency of the payload, while the crane model is performing a slewing action through $90^{\pm}$ and back every 8 seconds.

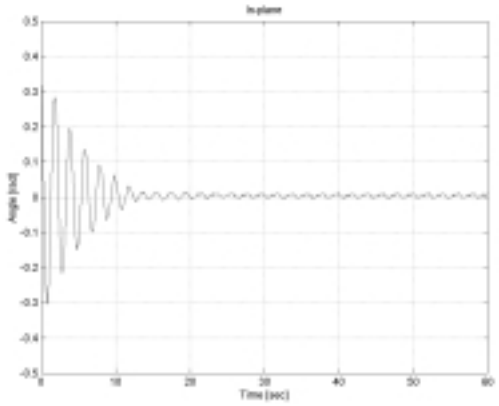

Figure 5.4: Experimental results: The in-plane angle of the payload cable as a function of time for the controlled case. Sinusoidal excitations in roll and pitch at the pendulation frequency of the payload sinusoidal excitation in heave at twice the pendulation frequency of the payload, and an initial disturbance of $20^{\pm}$ in the in-plane angle.

5.3 Experimental Setup for Tower Cranes

An experimental model of a tower crane was designed and built to validate the performance of the delayed-feedback control strategy on land-based cranes. The model crane has two degrees of freedom, a rotating jib on which a trolley can extend upto 1 m off the center of rotation of the jib, Fig 5.5. A rotary platform with a 1 : 45 gear ratio was used to give the crane its slewing degree of freedom. A ball screw with a pitch of 1=2 in was used to drive the trolley along the jib.

Both the rotational degree of freedom of the jib and the translational degree of freedom of the trolley are actuated using two brushless servo-motors. Optical encoders embedded within the servo-motors were used to obtain information about the translational and

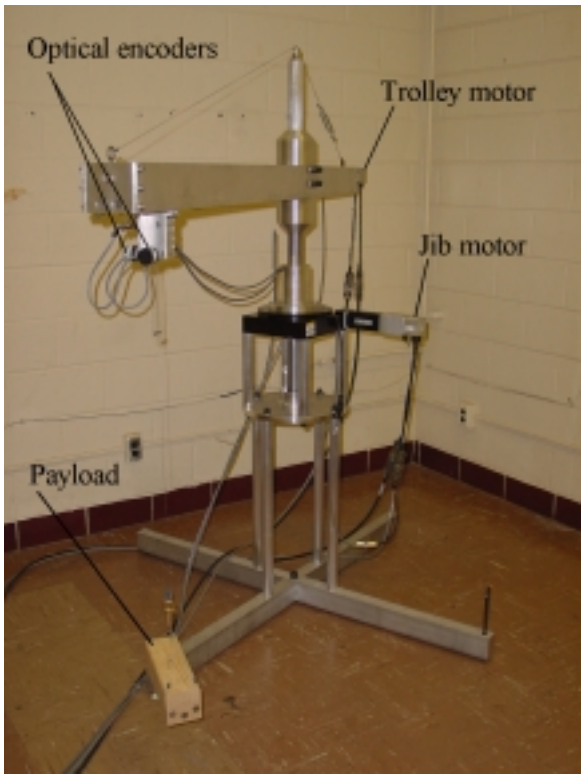

Figure 5.5: An experimental scale model of a tower crane.

rotational motion of the crane, Fig 5.5. Another set of two optical encoders placed at the suspension point of the hoisting cable were used to measure the in-plane and out-of-plane pendulation angles of the payload. A 1=24 scale model of an 8 ft by 8 ft by 20 ft container weighing 20 tons was used as a payload. The center of gravity of the payload was located 1 m below the boom tip. This length yields a pendulation frequency of 0:498 Hz.

A data acquisition board, similar to the one used earlier in the boom-crane setup, was added to a desktop computer. The board was used to sample the optical encoders of the crane and the payload hoisting cable. A C++ code was developed, which included the delayed-position feedback control algorithm, and was used to sample the data acquisition board registers and drive the amplifiers of the jib and the trolley actuators. The code is capable of turning the controller on and off at any time during the experiment.

5.4 Experimental Results for Tower Cranes

To obtain the maximum damping, the controller parameters used were a gain of 0:4 for both the in-plane and out-of-plane parts of the controller, and a time delay of 0:56 seconds for the in-plane and out-of-plane angles of the payload hoisting cable, which was about 0:28 of the natural pendulation period of the model payload.

Two sets of experiments were conducted. In both sets, controlled and uncontrolled cases were run. The first set of experiments was conducted for the rotary mode of operation. The trolley was placed at a radius of 40 in. The jib was then commanded to perform a rotation of $90^{\pm}$. The commanded motion consisted of a constant acceleration phase followed by a constant velocity phase and was terminated by a constant deceleration phase, Fig 5.6. In the uncontrolled case, as shown in Fig 5.7, the commanded motion

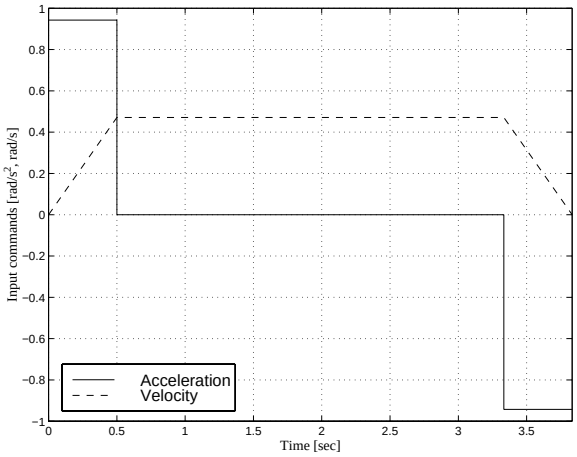

Figure 5.6: Commanded rotary motion.

caused the amplitude of the pendulation angles to grow rapidly in-plane and out-of-plane. These pendulations continued to exist during the commanded motion and after it was concluded. The same experiment was then repeated with the controller turned on. The commanded motion caused the out-of-plane pendulation angle to grow to nearly

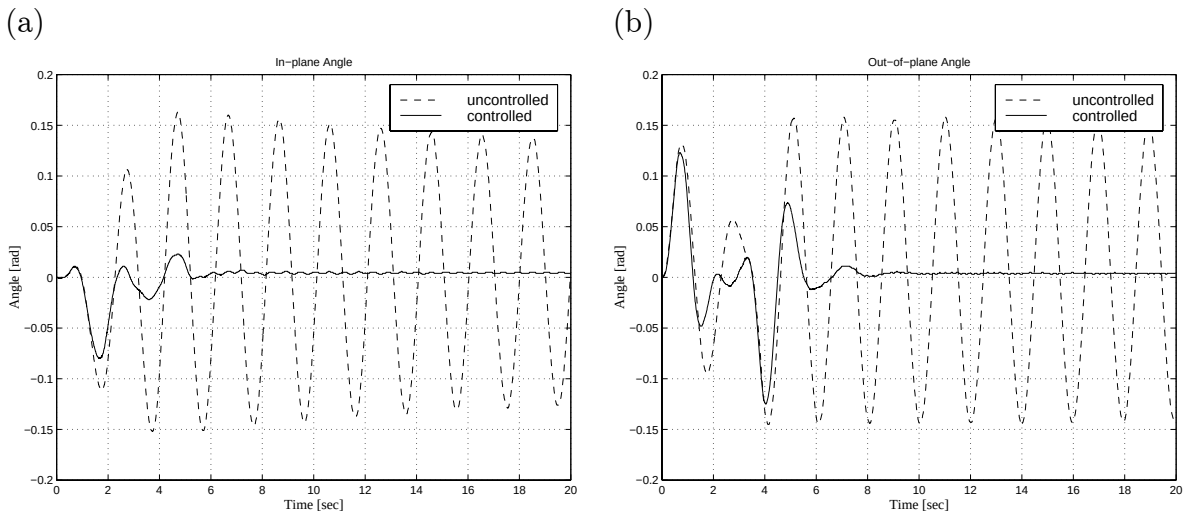

Figure 5.7: Experimental results for the rotary mode of operation: (a) in-plane and (b) out-of-plane angles of the payload cable as functions of time.

the same amplitude at the beginning of the acceleration and the deceleration phases. However, it dropped rapidly during the constant velocity phase as well as at the end of the commanded motion. On the other hand, the in-plane pendulation angle grew to a smaller amplitude at the beginning of the motion as a result of the centrifugal force on the payload, but was rapidly damped to a significantly smaller amplitude during the motion and virtually to zero shortly after the end of the commanded motion. Figure 5.8 shows the controlled and uncontrolled motions of the payload in the x- and y-coordinates. Although the controlled pendulation angles of the payload seamed to grow to an amplitude close to that of the uncontrolled case, the controlled motion of the payload had a smaller deviation from the desired motion than the uncontrolled motion.

In the second set of experiments, the crane was operated in the gantry mode; that is, the only commanded motion was a translational motion of the trolley. The trolley was placed at a radius of 10 in. The trolley was then commanded to move to a radius of 40 in. As in the rotary mode, the commanded motion consisted of a constant acceleration phase

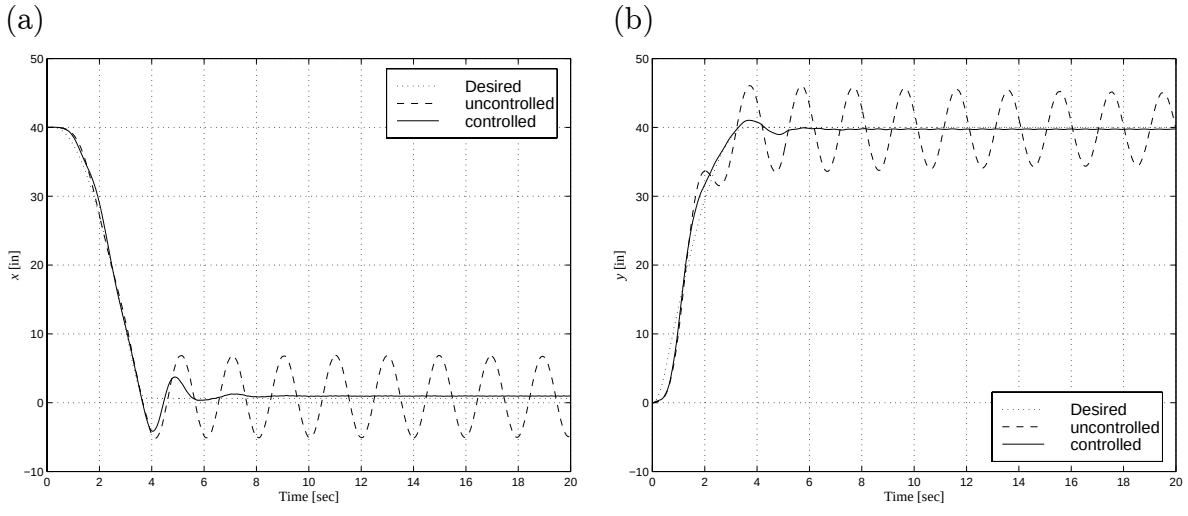

Figure 5.8: Experimental results for the rotary mode of operation: (a) x-motion and (b) y-motion of the payload as functions of time.

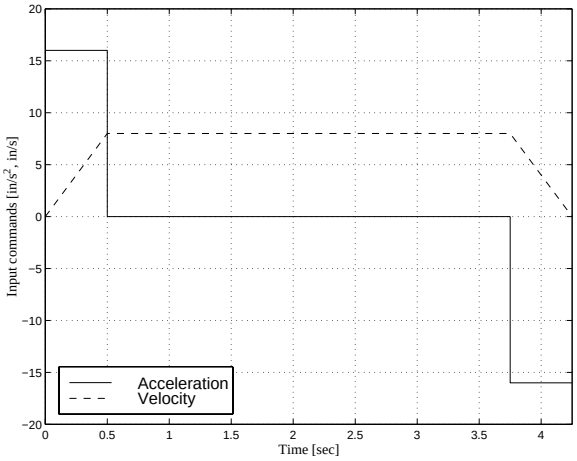

Figure 5.9: Commanded gantry motion.

followed by a constant velocity phase and was ended by a constant deceleration phase, Fig 5.9. In the uncontrolled case, as shown in Fig 5.10, the commanded motion caused the amplitude of the pendulation angles to grow. These pendulations continued to exist during the commanded motion and after it was concluded. The same experiment was then

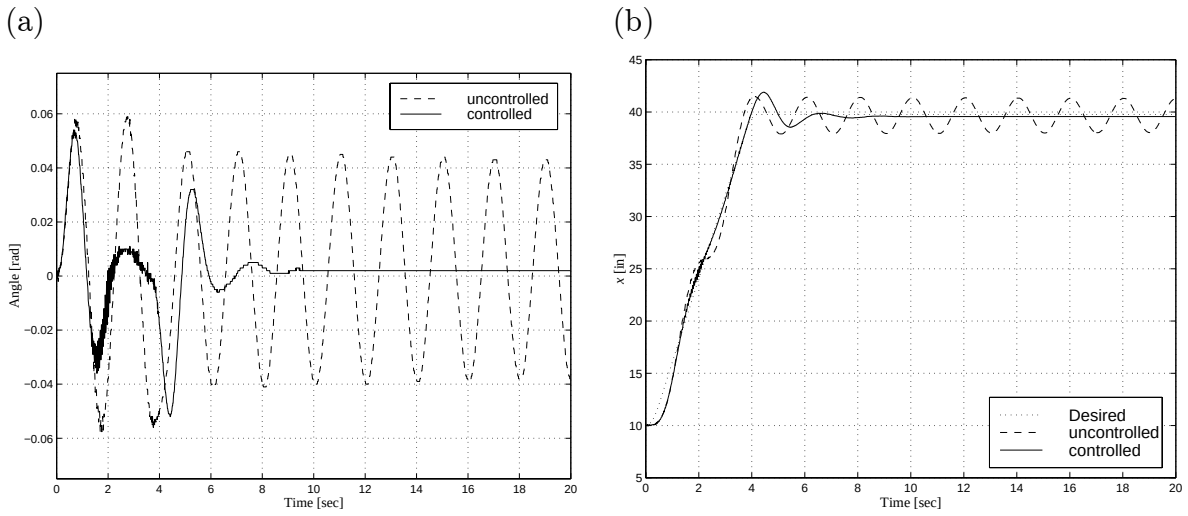

Figure 5.10: Experimental results for the gantry mode of operation: (a) pendulation angle of the payload cable and (b) payload motion as functions of time.

repeated with the controller turned on. The commanded motion caused the pendulation angle to grow to nearly the same amplitude at the beginning of the acceleration and deceleration phases, while in it dropped rapidly during the constant velocity phase as well as at the end of the commanded motion. Figure 5.10 also shows controlled and uncontrolled motions of the payload in the x-coordinate. The figure shows less deviation from the desired path of the payload and a faster drop in the pendulation at the end of the commanded motion.

An additional experiment was conducted, Fig 5.11. After the experiment was started, the payload was given in-plane and out-of-plane disturbances. The pendulation angles of the payload dropped in 5 seconds to less than $0{:}5^{\pm}$. Figure 5.12 shows the corresponding x- and y-motions of the payload as a result of the disturbances.

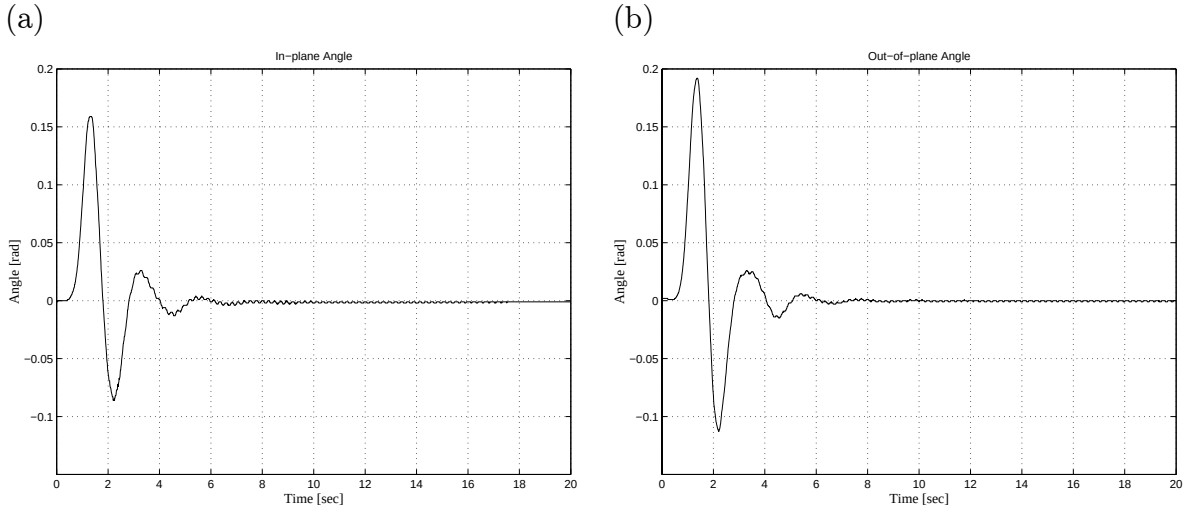

Figure 5.11: Experimental results: (a) in-plane and (b) out-of-plane angles of the payload cable as functions of time. The payload was given in-plane and out-of-plane initial disturbances.

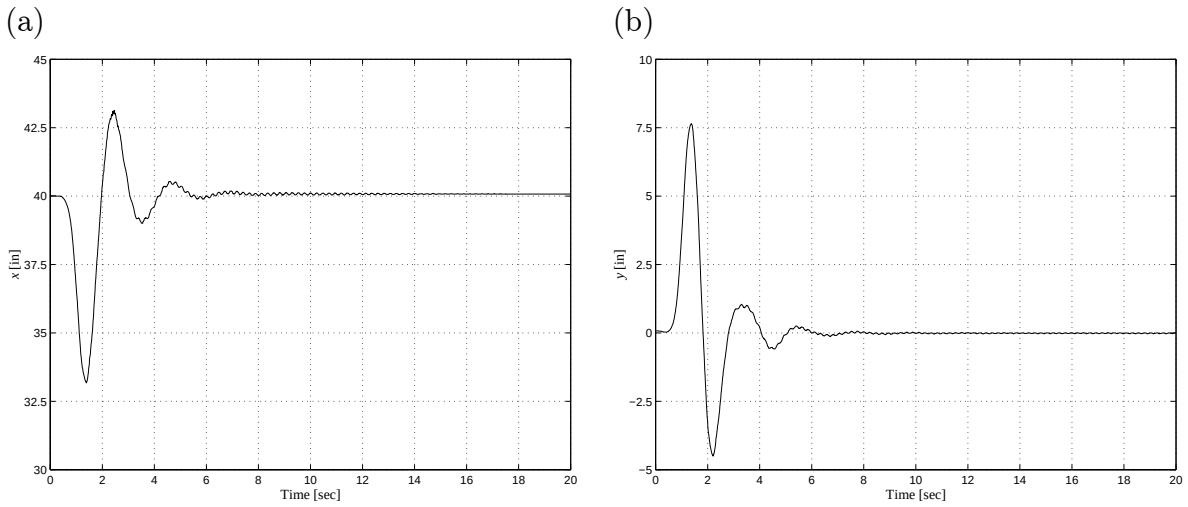

Figure 5.12: Experimental results: (a) x-motion and (b) y-motion of the payload as functions of time. The payload was given in-plane and out-of-plane initial disturbances.

Chapter 6

Conclusions

Delayed-position feedback together with luff-and-slew angle actuation is an effective method for controlling pendulations of cargo hoisted by ship-mounted cranes. Dramatic reductions in the pendulation angles of the payload in the controlled system were achieved in the numerical simulations as well as the experimental tests. The simulations and experimental results demonstrated the effectiveness and robustness of the proposed strategy against disturbances in the system.

The strategy was also applied and tested experimentally on a model of a land-based tower crane. The model was tested in both the rotary and gantry modes of operation. Although sizable pendulations were observed at the beginning and at the end of the commanded motions of the crane, the controller was clearly effective in absorbing these pendulations during and at the end of the commanded motions at high rates.

The large stable area in the gain-delay diagram allowed for flexible choices of the gain-delay combination. In ship-mounted boom cranes, where the motion of the boom of the

crane is restricted, smaller gains, although lead to slower damping, are more appreciable because they require less boom motion. On the other hand, in rotary and gantry cranes, where these restrictions on the motion of the suspension point of the payload hoisting cable are less severe, larger gains in the controller lead to a faster damping rate of the payload pendulations.

The delayed-position feedback controller shows clear effectiveness in absorbing base excitations, preventing payload pendulations due to these excitations and absorbing pre-existing pendulations. Although it was capable of handling and rapidly absorbing pendulations due to inertial forces resulting from the operator commands, the controller was not effective in preventing the initial and final pendulations of the hoisted payload due to the delayed reaction of the controller to these pendulations. However, one major advantage of the delayed-position feedback controller is in its algorithm. The structure of the control algorithm allows for an additional independent input; that is, the operator input. In this work, these inputs were raw acceleration commands. Before being introduced to the controller, the operator inputs can be preconditioned using a different controller. This controller would operate as a slave controller under the main delayed-position feedback controller. Both controllers working together would be very effective in preventing and absorbing pendulations at a high rate.

The mere fact that the delayed-position feedback controller accepts another controller in its algorithm without affecting its ability to absorb pendulations in the system is a great advantage to be explored for land-based cranes, which usually demand high accelerations and velocities. However, ship-mounted cranes are usually designed to move with lower accelerations and velocities, which require the controller to deal only with the payload pendulations due to the excitation resulting from the motion of the crane ship.

The cost effectiveness of the delayed-position feedback controller is another advantage.

The controller does not require any modifications to any crane structure. If required, these modifications would usually be very expensive, time consuming, and in some instances, impossible. A few sensors and a personal computer or a programmable control board are all that it takes to apply the controller.

A hybrid type controller with the delayed-position feedback controller as a master controller and an additional slave controller would be an excellent combination to solve the payload-pendulation problem of the different types of land-based cranes. This concept is now being investigated for land-based gantry cranes.

An automated soft-landing algorithm is now being developed for ship-mounted cranes. Combined with the delayed-position feedback controller, this algorithm will control the vertical position of the hoisted cargo to compensate for the changing relative vertical distance between the crane ship and the receiving vessel resulting from the heave motions of both vessels.

Bibliography

[1] Abdel-Rahman, E. M., and Nayfeh, A. H. "Cargo-Pendulation Reduction in Boom Cranes via Cable-Length Manipulation". Proceedings of the 41th AIAA Structure Dynamics and Material Conference, AIAA-2000-1541, 2000.

[2] Alsop, C. F., Forster, G. A., and Holmes, F. R. "Ore Unloader Automation - A Feasibility Study". Proceedings of IFAC on Systems Engineering for Control Systems, pages 295–305, 1965.

[3] Balachandran, B., and Li, Y. "A Mechanical Filter Concept to Suppress Crane Load Oscillations". Proceedings of the DETC'97 ASME Design Engineering Technical Conferences, DETC97/VIB-4091, 1997.

[4] Balachandran, B., Li, Y., and Fang, C. "A Mechanical Filter Concept for Control of Non-Linear Crane-Load Oscillations". Journal of Sound and Vibration, 228(3):651–682, 1999.

[5] Burg, T., Dawson, D., Rahn, C., and Rhodes, W. "Nonlinear Control of an Overhead Crane via the Saturating Control Approach of Teel". Proceedings of the 1996 IEEE International Conference on Robotics and Automation, pages 3155–3160, 1996.

[6] Carbon, L. "Automation of Grab Cranes". Siemens Review XLIII, 2:80–85, 1976.

[7] Chin, C., Nayfeh, A. H., and Abdel-Rahman, E. "Nonlinear Dynamics of a Boom Crane". Journal of Vibration and Control, in press, 2000.

[8] d'Andrea-Novel, B., and Levine, J. "Modeling and Nonlinear Control of an Overhead Crane". Proceedings of the International Symposium MTNS-89, 2:523–529, 1989.

[9] Elling, R. E., and McClinton, A. T. "Dynamic Loading of Shipboard Cranes". Ocean 1973 IEEE International Conference on Engineering in the Ocean Environment, pages 174–177, 1973.

[10] Fossen, T. I. "Guidance and Control of Ocean Vehicles". John Wiley and sons, Chichester, England, 1994.

[11] Golafshani, A. R., and Aplevich, J. D. "Computation of Time-Optimal Trajectories for Tower Cranes". Proceedings of the IEEE Conference on Control Applications, pages 1134–1139, 1995.

[12] Gustafsson, T. "Modelling and Control of a Rotary Crane". Proceedings of the 3rd European Control Conference, pages 3805–3810, 1995.

[13] Hara, K., Tetsuhiko, T., Kobayashi, A., and Okamoto, M. "Jib Crane Control to Suppress Load Swing". International Journal of Systems Science, 20(5):715–731, 1989.

[14] Hubbell, J. T., Koch, B., and McCormick, D. "Modern Crane Control Enhancements". Posrts'92, pages 757–767, 1992.

[15] Imazeki, M., Mutaguchi, M., Iwasaki, I., and Tanida, K. "Active Mass Damper for Stabilizing the Load Suspended on a Floating Crane". IHI Engineering Review, 31(2):61–69, 1998.

[16] Ito, H., Senda, Y., and Fujimoto, H. "Dynamic Behavior of a Load Lifted by a Mobile Construction-Type Crane". Bulletin of JSME, 21(154):600–608, 1978.

[17] Iwasaki, I., Tanida, K., Kaji, S., and Mutaguchi, M. "Development of an Active Mass Damper for Stabilizing the Load Suspended on a Floating Crane". Proceedings of the ASME Design Engineering Technical Conference, DETC97/VIB-3816, 1997.

[18] Kimiaghalam, B., Homaifar, A., and Bikdash, M. "Fuzzy Dynamic Friction Controller for a Ship Crane". Proceedings of the 6th International Conference on Fuzzy Theory and Technology, 1:203–206, 1998.

[19] Kimiaghalam, B., Homaifar, A., and Bikdash, M. "Pendulation Suppression of a Shipboard Crane Using Fuzzy Controller". Proceedings of the American Control Conference, pages 586–590, 1999.

[20] Kimiaghalam, B., Homaifar, A., and Bikdash, M. "Feedback and Feedforward Control Law for a Ship Crane With Maryland Rigging System". Proceedings of the American Control Conference, 2000.

[21] Koscielny, R., and Wojciech, S. "Nonlinear Vibration of the Subsystem in Various Media Conditions". Structural Dynamics and Vibration, 63:47–52, 1994.

[22] Kral, R., Kreuzer, E., and Wilmers, C. "Nonlinear Oscillations of a Crane Ship". Z. Angew Math. Mech., 76(S4):5–8, 1996.

[23] Lewis, D., Parker, G. G., Driessen, B., and Robinett, R. D. "Command Shaping Control of an Operator-in-the-Loop Boom Crane". Proceedings of the American Control Conference, pages 2643–2647, 1998.

[24] Li, Y., and Balachandran, B. "Mechanical Filters for Control of Crane-Load Oscillations". Proceedings of the MURI on Nonlinear Active Control of Dynamical Systems, 1999.

[25] McCormick, F. J., and Witz, J. A. "An Investigation into the Parametric Excitation of Suspended Loads During Crane Vessel Operations". Underwater Technology, V, 19:30–39, 1993.

[26] Miles, J. W. "Stability of Forced Oscillations of a Spherical Pendulum". Quart. Appl. Math., V, 20:21–32, 1962.

[27] Miles, J. W. "Resonant Motion of a Spherical Pendulum". Physica D, 11D(3):309–323, 1984.

[28] Nojiri N., and Sasaki, T. "Motion Characteristics of Crane Vessels in Lifitng Operation". Proceedings of the 15th Annual O®shore Technology Conference, OTC 4603, 1983.

[29] Osinski, M., and Wojciech, S. "Dynamics of Hoisting Appliances in Maritime Conditions". Machine Vibration, 3:76–84, 1994.

[30] Osinski, M., and Wojciech, S. "Application of Nonlinear Optimisation Methods to Input Shaping of the Hoist Drive of an Off-Shore Crane". Nonlinear Dynamics, 17:369–386, 1998.

[31] Parker, G. G., Groom, K., Hurtado, J. E., Feddema, J., Robinett, R. D., and Leban, F. "Experimental Verification of a Command Shaping Boom Crane Control System". Proceedings of the American Control Conference, pages 86–90, 1999.

[32] Parker, G. G., Petterson, B., Dohrmann, C. R., and Robinett, R. D. "Command Shaping For Residual Vibration Free Crane Maneuvers". Proceedings of the American Control Conference, pages 934–938, 1995.

[33] Parker, G. G., Petterson, B., Dohrmann, C. R., and Robinett, R. D. "Vibration Suppression of Fixed-Time Jib Crane Maneuvers". Proceedings of the SPIE Smart Structures and Materials Conference, 2447:86–90, 1995.

[34] Patel, M., Brown, D., and Witz, J. "Operability Analysis for a Monohull Crane Vessel". Transaction of the Royal Institute of Naval Architects, 129:103–113, 1987.

[35] Posiadala, B. "Effect of Vibration in Hoist System on Dynamics of Truck Crane". Z. Angew Math. Mech., 76(S5):403–404, 1996.

[36] Posiadala, B. "Influence of Crane Support System on Motion of the Lifted Load". Mechanism and Machine Theory, 32:9–20, 1997.

[37] Posiadala, B., Skalmierski, B., and Tomski, L. "Motion of the Lifted Load Brought by a Kinematic Forcing of the Crane Telescopic Boom". Mechanism and Machine Theory, 25:547–556, 1990.

[38] Posiadala, B., Skalmierski, B., and Tomski, L. "Vibration of Load Lifted by a Truck Crane with Consideration of Physical Properties of Rope". Machine Dynamics Problems, 2:85–104, 1991.

[39] Rawston, P. J., and Blight, G. J. "Prediction of Weather Fowntime for Derrick Barges". Proceedings of the 10th Annual O®shore Technology Conference, OTC 3150, 1978.

[40] Sakawa, Y., and Nakazumi, A. "Modeling and Control of a Rotary Crane". Transactions of the ASME Journal of Dynamic Systems, Measurement, and Control, 107:200–206, 1985.

[41] Sakawa, Y., Shindo, Y., and Hashimoto, Y. "Optimal Control of a Rotary Crane". Journal of Optimization Theory and Applications, 35(4):535–557, 1981.

[42] Sato, K., and Sakawa, Y. "Modeling and Control of a Flexible Rotary Crane". International Journal of Control, 48(5):2085–2105, 1988.

[43] Schellin, T. E., Jiang, T., and Sharma, S. D. "Crane Ship Response to Wave Groups". Journal of O®shore Mechanics and Arctic Engineering, 113:211–218, 1991.

[44] Schellin, T. E., Sharma, S. D., and Jiang, T. "Crane Ship Response to Regular Waves: Linearized Frequency Domain Analysis and Nonlinear Time Domain Simu-

lation". Proceedings of the 8th International Conference on O®shore Mechanics and Arctic Engineering, ASME, II:627–635, 1989.

[45] Souissi, R., and Koivo, A. J. "Modeling and Control of a Rotary Crane for Swing-Free Transport of Payloads". First IEEE conference on Control Applications, 2:782–787, 1992.

[46] Todd, M. D., Vohra, S. T., and Leban, F. "Dynamical Measurements of Ship Crane Load Pendulation". Oceans '97 MTS/IEEE Conference Proceedings, 2:1230–1236, 1997.

[47] Towarek, Z. "The Dynamic Stability of a Crane Standing on Soil During the Rotation of the Boom". International Journal of Mechanical Sciences, 40:557–574, 1998.

[48] Vaughers, T. "Joint Logistics Over the Shore Operations". Naval Engineers Journal, 106(3):256–263, 1994.

[49] Vaughers, T., and Mardiros, M. "Joint Logistics Over the Shore Operations in Rough Seas". Naval Engineers Journal, pages 385–393, 1979.

[50] Wen, B., Homaifar, A., Bikdash, M., and Kimiaghalam, B. "Modeling and Optimal Control Design of Shipboard Crane". Proceedings of the American Control Conference, pages 593–597, 1999.

[51] Wen, B., Kimiaghalam, B., Homaifar, A., and Bikdash, M. "Modeling and Control of a Shipboard Crane". Proceedings of the world automation Congress, 2000.

[52] Witz, J. "Parametric Excitation of Crane Loads in Moderate Sea States". Ocean Engineering, 22:411–420, 1995.

[53] Yuan, G. H., Hunt, B. R., Grebogi, C., Ott, E., Yorke, J. A., and Kostelich, E. J. "Design and Control of Shipboard Cranes". Proceedings of the DETC'97 ASME Design Engineering Technical Conferences, DETC97/VIB-4095, 1997.

Vita

Ziyad Nayif Masoud was born on October 23, 1969 in Beirut, Lebanon. In 1975 he and his family moved to Benghazi, Libya where he attended school and graduated with a Bachelor's degree in Mechanical Engineering from Garyounis University in 1991. In 1992 he moved to Amman, Jordan and attended Jordan University and graduated with a Master's degree in Mechanical Engineering. Ziyad joined Virginia Tech in 1998 to pursue his Ph.D. degree.